Comparison of conditioning factors classification criteria in large scale statistically based landslide susceptibility models

Marko Sinčić[1], Sanja Bernat Gazibara[1], Mauro Rossi[2], Snježana Mihalić Arbanas[1]

[1]Faculty of Mining, Geology and Petroleum Engineering, University of Zagreb, Pierottijeva 6, 10000 Zagreb, Croatia
[2]Consiglio Nazionale delle Ricerche, Instituto di Ricerca per la Protezione Idrogeologica, via Madonna Alta 126, 06128 Perugia, Italy

Correspondence to: Marko Sinčić (msincic@rgn.hr)

Abstract. The large scale landslide susceptibility assessment (LSA) is an important tool for reducing landslide risk through the application of resulting maps in spatial and urban planning. The existing literature more often deals with LSA modelling techniques and the scientific research very rarely focuses on acquiring relevant thematic and landslide data, necessary to achieve reliable results. Therefore, the paper focuses on the crucial step of classifying continuous landslide conditioning factors for susceptibility modelling by presenting an innovative comprehensive analysis that resulted in 54 landslide susceptibility models to test 11 classification criteria (scenarios which vary from stretched values, partially stretched classes, heuristic approach, classification based on studentized contrast and landslide presence, and commonly used classification criteria, such as Natural Neighbor, Quantiles and Geometrical intervals) in combination with five statistical methods. The large scale landslide susceptibility models were derived for small and shallow landslides in the pilot area (21 km^2) located in the City of Zagreb (Croatia), which occur mainly in soils and soft rocks. Some of the novelties in LSA are the following: scenarios using stretched landslide conditioning factor values or classification with more than 10 classes prove more reliable; certain statistical methods are more sensitive to the landslide conditioning factor classification criteria than others; all the tested machine learning methods give the best landslide susceptibility model performance using continuously stretched landslide conditioning factors derived from high-resolution input data. The research highlights the importance of qualitative assessments, alongside commonly used quantitative metrics, to verify spatial accuracy and to test the applicability of derived landslide susceptibility maps for spatial planning purposes.

1 Introduction

Addressing landslide hazard is commonly done by zoning, i.e. deriving landslide susceptibility, hazard, and risk zoning maps (Corominas et al., 2014). Brabb, (1984) defined landslide susceptibility as a 'likelihood of a landslide occurring in a given area', indicating the spatial component exclusively. In the years to come, Soeters and van Westen, (1996), Guzzeti et al., (1999), van Westen et al., (2008), Fell et al., (2008a,b), Corominas et al., (2014), and Reichenbach et al., (2018) represent some of the most significant progress done in the field of research considering landslide susceptibility. One of the most popular approaches to derive landslide susceptibility models (LSM) is using statistical methods, where the most recent and detailed

review of statistically based landslide susceptibility models is given in Reichenbach et al., (2018), whereas Merghadi et al., (2020) emphasize only machine learning methods by reviewing algorithm performance. Literature (e.g. van Westen et al., 2008 and Corominas et al., 2014) has shown two main groups of data needed for applying statistical methods in landslide susceptibility assessments (LSA), i.e. landslide inventory maps and landslide conditioning factors (LCFs). Moreover,

35 Reichenbach et al., (2018) identified acquiring relevant landslide and thematic information (i.e. LCF) as the first two steps for preparing a LSA. Many papers discuss different methods (e.g. Wang et al., 2016a, Chen et al., 2017, Merghadi et al., 2020), mapping units (e.g. Bornaetxea et al., 2018, Jacobs et al., 2020), inventory types (e.g. Guzzetti et al., 2012, Petschko et al., 2015) and the importance and/or selection of LCFs (Donati and Turrini, 2002, Jebur et al., 2014, Gaidzik and Ramírez, 2021), which are all necessary steps in LSA according to Reichenbach et al., (2018).

40 This research is situated in the European Panonnian Basin, i.e. in the City of Zagreb in hilly regions of the southern foothills of Medvendica Mt., which are susceptible to sliding. Despite long-term investigation on landslide phenomena, Jurak et al., (1996) and Mihalić, (1998) identified the lack of sustainable landslide inventories and landslide hazard maps as the main issue in the landside risk management in the Republic of Croatia. As a result, a landslide inventory map (Bernat Gazibara et al., 2019a) and a landslide susceptibility map (Bernat Gazibara et al., 2023) were derived, followed by emphasizing the importance

45 and necessity of large scale landslide susceptibility maps in the system of spatial and urban planning (Mihalić Arbanas et al., 2023). Regardless of the degree of urbanization, landslide occurrence is commonly related to geomorphological, geological and climate settings, as well as anthropogenic factors. Furthermore, Bernat Gazibara et al., (2017) indicate that the main landslide triggers in the area are precipitation and snow melting, i.e. long continuous precipitation periods or short precipitation periods of high intensity. The input data for LSA in this study were successfully acquired during previous research

50 investigations in the study area (e.g. Bernat Gazibara et al., 2017, Bernat Gazibara et al., 2019a, Bernat Gazibara et al., 2023), and past large scale assessment in Croatia (Sinčić et al., 2022a), but their optimal application in landslide susceptibility modelling remained an open question. The relevance and new insight on acquiring input data for preparing LCFs on a large scale (i.e. 1:5 000) were provided by Sinčić et al., (2022a) and proved by analyzing the predictive performances of large scale LSA by Krkač et al., (2023).

55 This relevant aspect of LSA was addressed by Jebur et al., (2014), which used Weight of Evidence (WoE), Logistic Regression (LR) and Support Vector Machine (SVM) methods in a large scale case study to compare a LiDAR derived LCF set with a set containing additional LCFs such as land use and geology. AUC comparison between the two scenarios favored LiDAR only derived LCFs, addressing the amount and type of LCFs used in the research, but not their classification criteria. Similarly, Dou et al., (2015) applied LR and Statistical Index methods to demonstrate that six LCFs with high correlation to landslide

60 occurrence result in better success and prediction rate than a complete set of 15 LCFs. Donati and Turrini, (2002) show that when using categorical LCFs, only a few classes can significantly influence the LSA, confirming the importance of how LCFs are classified. These studies showed the need for relevant LCF acquisition and selection criteria, whereas the Leave One Out test available in LAND-SUITE software (Rossi et al., 2022), certainty factor models (Dou et al., 2015), and variable importance (Shirvani, 2020) are some methods used for LCF selection.

65 LCF classification issues were discussed by Yan et al., (2019), who defined two classification criteria for LCFs selected by reviewing classification criteria in different studies available in the literature. Specifically, the two classification criteria for each of the five LCF results with fewer or more classes used to develop 32 LSM scenarios to test all the combinations. From the 32 derived maps, a low difference of 0.03 AUC between minimum and maximum AUC was identified. Namely, the best result was obtained when all LCFs were used in a scenario that included more classes in most LCFs. Xiao et al., (2021)

70 implemented a different strategy, aimed to reduce local correlations among LCFs by reclassifying them to increase LSA accuracy. As stated by Bonham-Carter et al., (1990) and Neuhäuser and Terhorst, (2007), contrast or studentised contrast (C_{st}) metrics can be used to determine classification cut-off values in continuous LCFs when using a bivariate approach such as WoE or Information Value (IV). Moreover, generalizing continuous LCFs enables maximized spatial relations and statistical robustness (Neuhäuser et al., 2012). Concretely, Mathew et al., (2007) used the C_{st} curve maximum to split the distance to

75 roads, drainage, and lineament LCFs into two classes. Furthermore, Neuhäuser et al., (2012) applied the C_{st} curve in the WoE method to convert continuous LCFs to categorical by observing maximum and local maximum C_{st} values. Jebur et al., (2014) used mainly the quantile criteria to derive ten classes for stretched rasters and a heuristic approach for buffer zones from vector lines (i.e. proximities or distances). On the other hand, Yusof et al., (2015) applied only the quantile criteria to classify LCFs into ten classes, based on the approach by Tehrany et al., (2013) and Tehrany et al., (2014) in flood susceptibility mapping.

80 Huang et al., (2020a,b) and Huang et al., (2022) applied the natural breaks classification criteria and defined eight classes in each LCF. Wang et al., (2016b), Cui et al., (2017), Zhao and Chen, (2020), and Wang et al., (2020) used what seems to be equal intervals defined heuristically without specifications, whereas Wang et al., (2021) did not classify continuous LCFs and applied them as stretched rasters in the analysis. Several papers dealing with large scale LSA (e.g. Vojteková and Vojtek, 2020 and Xing et al., 2021) also do not specify the classification criteria but present the LCFs with popular equal interval classes

85 likely defined heuristically. Similarly, Wang et al., (2016b) used equal intervals to classify slope and buffer zones for LCFs, whereas a heuristic approach was selected for stretched rasters. In most of the mentioned studies, which applied a heuristic approach, a relatively low number of classes in LCFs are often defined, i.e. from 4 to 6 classes. A detailed comparison of all these criteria and techniques is still missing, especially on large scale assessments and with adequate metrics. Based on the latter, and as confirmed by Huang et al., (2020b) and Xing et al., (2021), there is no uniform approach to classifying continuous

90 LCFs. It can be concluded that no systematic analysis to compare the criteria was done, as the researchers are instead applying what was already confirmed successful in different individual case studies.

Few papers deal with LCF processing once they are selected, i.e. discussing the process of classifying continuous LCFs (e.g. Yan et al., 2019, Xiao et al., 2021), which is the scope of this study. Therefore, this paper compares 11 criteria used to define the processing of continuous LCFs, i.e. transform relevant input data layers into LCFs suitable for application in landslide

95 susceptibility modelling. Unlike Yan et al., (2019), which are more oriented into case study combinations of LCFs with different derived LCF classes, we aim to develop a uniform approach for classifying continuous LCFs, leading to defining a first step for large scale LSA methodology. Besides testing the 11 scenarios where continuous LCFs are categorized, each scenario is applied in five statistical landslide susceptibility methods, including IV, Logistic Regression (LR), Neural Network

(NN), Random Forests (RF), and SVM. Such methods were considered to analyze the influence of LCF classification criteria on LSA accuracy using different statistical modelling approaches, and they were selected because they are commonly used in LSA (Reichenbach et al., 2018).

Remote sensing has proven helpful for LSA, leading to better landslide hazard mitigation strategies. Concretely, different remote sensing techniques are widely applied for data acquisition when studying landslide hazard, as presented by Scaioni et al., (2014) and Ray et al., (2020), whereas in this paper, geomorphological and hydrological LCFs are based on LiDAR (Light Detection and Ranging) point cloud data acquired with Airborne Laser Scanning (ALS). Furthermore, the landslide inventory map was derived by mapping on morphometric maps derived from a high-resolution DTM (Digital Terrain Model), which shows a significant advantage compared to other methods for mapping small landslides under vegetation (Razak et al., 2013, Bernat Gazibara et al., 2019a). Jebur et al., (2014) argue that LiDAR-derived LCFs could be sufficient for LSA where geological LCFs (e.g. soil and geology) are not available, whereas Sinčić et al., (2022a) were able to derive a complete set of LCFs together with a set of elements at risk for large scale LSA by using exclusively high-resolution LiDAR and orthophoto data in combination with publicly available small scale geological data.

Besides a study case presented by Yusof et al., (2015) using LR and Evidential Belief Function, comparing LSA methods on a large scale is not common in the literature. Hence, one of the novelties of this paper is presenting a detailed comparison, including the quantitative and qualitative perspective of five popular LSA methods applied on a large scale with relevant input data of high spatial accuracy. Zêzere et al., (2017) point out that the best AUC metric values do not necessarily define the best LSM. Similarly, Vakhshoori and Zare, (2018) emphasize that AUC values might be deceiving or ineffective in detecting uncertainties in spatial prediction and can only indicate general reliability. To address the issue, Vakhshoori and Zare, (2018) suggest studying additional metrics, such as Cohen's kappa, to acquire additional information about the LSM. Considering the susceptibility quality level (SQL) introduced by Guzzetti et al., (2006a,b), Reichenbach et al., (2018) identified a low amount of papers published with a high SQL rank. Addressing model fitting and predictive performance and measuring uncertainties in the derived models, 54 LSMs based on combinations of five methods (IV, LR, RF, NN, SVM) and 11 LCF classification criteria derived in this paper are considered high SQL, ensuring systematical and unbiased comparison. Moreover, researching the application of LSMs in spatial planning (Mihalić Arbanas et al., 2023), we qualitatively present derived LSMs in close up views and high resolution to measure the applicability of the used zonation method, i.e. determine visually susceptibility class area distribution. However, choosing the optimal zonation method is out of the scope of this study, and the one presented in this paper serves exclusively for uniform comparison of derived LSMs. Moreover, it should be stated that optimization of used statistical methods is a topic beyond the objective of this research. We argue that large scale LSA using high quality input data should also be measured qualitatively as expert judgement by observing real environmental conditions on high resolution DTM derivatives. It provides necessary insight into map quality and applicability, which is not detected by commonly used quantitative approaches (e.g., AUC).

2 Materials

2.1 Study area

The study area is located in the City of Zagreb, the capital of Croatia, in the northwest part of the country. It encompasses 21 km^2 of the southern slopes of the Medvednica mountain, i.e. the western part of the Podsljeme area. The City of Zagreb
135 belongs to the European Pannonian Basin, whereas the Podsljeme area encompassing the study area is depicted with hilly relief, with 90% of the study area steeper than 5° (Bernat Gazibara et al., 2019b). Basic geological settings can be described as upper Miocene and Quaternary sediments making up 92% of the study area, described in detail in the geological map 1:100 000 and supplementary geological notes developed by Šikić et al., (1972) and Šikić et al., (1979), respectively. With a dense population and a high degree of urbanization, which is increasing, the Podsljeme area has been under research regarding
140 landslide phenomena in the last 50 years, starting with the first landslide inventory map by Šikić, (1967), and following geomorphological landslide maps from 1979 (Polak et al., 1979) and a geomorphological inventory from 2006 (Miklin et al., 2006). More recently, Bernat Gazibara et al., (2014a,b) described landslide events triggered by intensive rainfall. Moreover, Mihalić Arbanas et al., (2016) identified the lack of a suitable landslide inventory as one of the critical issues in landslide risk management in the City of Zagreb. As a result, a LiDAR based landslide inventory map for the 21 km^2 in this study area was
145 derived (Bernat Gazibara et al., 2019a,b), followed by a susceptibility assessment (Bernat Gazibara et al., 2023). Satisfactory results were obtained, confirming the proposed methodology for large scale LSA. Considering the highly urbanised environment, population density and a continuous increase of human induced landslides in the Podsljeme area (Jurak et al., 2008 and Mihalić Arbanas et al., 2014), a large scale landslide susceptibility assessment is necessary for adequate landslide management in the study area.

150 ### 2.2 Input data

The first landslide inventory map developed from LiDAR data for the study area was completed by Bernat Gazibara et al., (2019a,b) based on ALS, which was performed during the leaf-off period in Croatia in 2013. Furthermore, another LiDAR ALS was performed in 2020 (Bernat Gazibara et al., 2022, Bernat Gazibara et al., 2023) to verify the existing landslide inventory map, providing a multi-temporal insight into landslide occurrence. Namely, the landslide inventory map consists of
155 702 mapped polygons, with the most frequent landslide area being 400 m^2 and a density of 33 landslides per square kilometre. The input data layers needed to derive LCFs are prepared from source data, and are classified according to their origin in continuous and categorical, as presented in Table 1. Furthermore, continuous input data layers can be subdivided into vector lines (e.g. geological contacts, faults, drainage network, all streams) and stretched rasters (e.g. elevation, slope, terrain wetness). On the other hand, lithology (rock type) and land use made up the polygon group of categorical input data layers,
160 unlike aspect being the only categorical raster type. Continuous stretched rasters are presented with edge values (Fig. 1a, b, e), whereas categorical input data layers are depicted with their classes (Fig. 1c, d, g). Furthermore, the continuous line input data layers' spatial presence is illustrated in Fig. 1d, e, f.

Table 1 Overview of source data used for derivation of input data layers

Source Data	Scale	Input data layer	Obtained by	Categorization
LiDAR point cloud	5 m resolution	Elevation	Interpolation	Continuous stretched raster
		Slope	ArcGIS 10.8 Slope tool	Continuous stretched raster
		Aspect	ArcGIS 10.8 Aspect tool	Categorical (classified) raster
		Terrain wetness	Evans et al., (2014)	Continuous stretched raster
		Drainage network	ArcGIS 10.8 Spatial Analyst Toolbox	Continuous line (vector)
Croatian Basic Geological Map	1:100 000	Lithology (rock type)	Digitization	Categorical polygon (vector)
		Geological contact	Digitization	Continuous line (vector)
		Faults	Digitization	Continuous line (vector)
Topographic Map of Croatia	1:25 000	Streams	Digitization	Continuous line (vector)
Land use planning maps	Large scale	Land use	City of Zagreb (2011)	Categorical polygon (vector)

165

We note that the used geological input data is small scale, but considering preliminary analysis in the LCF selection process, it resulted in being more relevant to landslide occurrences in terms of the leave one out test in comparison to the alternative geological map in scale 1:5 000. Furthermore, the mentioned small scale geological input data was also applied in Bernat Gazibara et al., (2023) where it yielded excellent results.
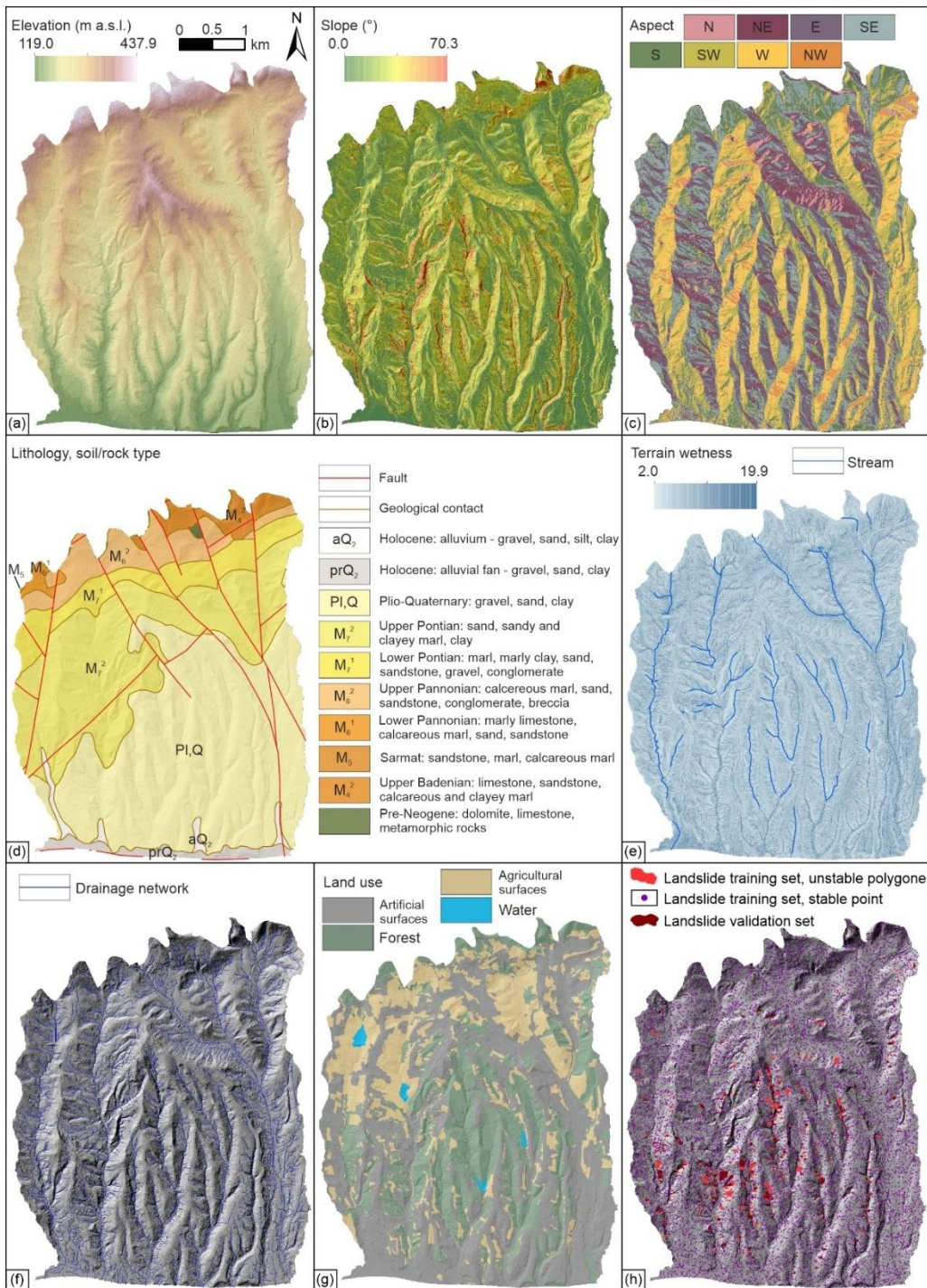
Figure 1 Input data layers for landslide susceptibility analyses: (a) elevation; (b) slope; (c) aspect; (d) lithology (soil/rock type), geological contact and faults; (e) terrain wetness and streams; (f) drainage network; (g) land use; (h) landslide dataset

3 Methodology

3.1 Preparing input data

Categorical LCFs (aspect, lithology, land use) are equivalent to input data layers presented in Table 1 and were used equally in all 11 scenarios, an exception being aspect in scenario S11, as explained further in the section. Classes in categorical LCFs were ordered according to frequency ratio values defined by the presence of an unstable training landslide set. Continuous LCFs were derived differently from input data layers (Table 1, Fig. 1), as follows for 11 scenarios and briefly summarized in Table 2.

Table 2 Summary of 11 defined scenarios considering different categorization criteria

Scenario	Description of categorization criteria	
	Stretched rasters	**Line vector**
S1	100 equal classes	100 equal buffer zones
S2	50 equal classes	50 equal buffer zones
S3	Heuristic classification based on researcher experience	
S4	Studentized contrast defined on S1 classes, positive and negative segments	
S5	Studentized contrast defined on S1 classes, positive segments split into two, negative segments	
S6	Studentized contrast defined on S1 classes, positive segments split into two, negative segments split into two	
S7	Classification based on landslide density in S1 classes, i.e. expected vs. mapped landslide area	Classification based on landslide density in S1 classes, equation (4)
S8	10 Natural Breaks (NB) classification method applied on input data layers (stretched raster)	10 Natural Breaks (NB) classification method applied on scenario S1 classes
S9	10 Quantile (Q) classification method applied on input data layers (stretched raster)	10 Quantile (Q) classification method applied on scenario S1 classes
S10	10 Geometrical Interval (GI) classification method applied on input data layers (stretched raster)	10 Geometrical Interval (GI) classification method applied on scenario S1 classes
S11	Input data layers (stretched raster)	Scenario S1 classes

Continuous stretched rasters (elevation, slope, terrain wetness) were reclassified into 100 equal classes for scenario S1. Regarding continuous line vector LCFs (geological contact, faults, drainage network, all streams), 100 equal multiple buffer ring zones were derived to finalize scenario S1 LCFs (Fig. 2a). Similarly to scenario S1, scenario S2 is defined by 50 equal classes, as illustrated in Fig. 2b. The aim of defining scenarios S1 and S2 is to simulate the continuous input data layer to a high and low detailed extent, respectively. In Scenario S3, LCFs were defined by heuristically classifying and defining buffer zones for continuous rasters and line input data layers, respectively. The subjective approach was led by researchers' experience (e.g. Sinčić et al., 2022b, Krkač et al., 2023) and previous work in the study area (e.g. Bernat Gazibara et al., 2023).

For each of the 100 scenario S1 LCF classes, C_{st} values were calculated based on the bivariate approach, i.e. observing class pixel size and landslide pixels presence in the class. Namely, C_{st} is defined as a ratio of contrast (C) to its standard deviation $s(C)$ (Bonham-Carter, 1994), i.e.:

$$C_{st} = \frac{C}{s(C)} \tag{1}$$

where,

$$C = W^+ - W^- \tag{2}$$

where W^+ and W^- indicate positive and negative weight factors in the WoE method, respectively. Standard deviation $s(C)$ is defined as:

$$s(C) = \sqrt{S(W^+)^2 + S(W^-)^2} \tag{3}$$

where $S(W^+)^2$ and $S(W^-)^2$ are variances of weights defined by Bishop et al., (1975). The C_{st} curve was defined for each LCF, followed by observing positive and negative C_{st} trends throughout the 100 classes. Cut-off lines for scenario S4 were determined by dividing the C_{st} curve into positive and negative segments, as depicted in Fig. 2c. To define scenario S5, each scenario S4 positive segment was split into two by defining an additional cut-off line at the highest peak point (Fig. 2d).
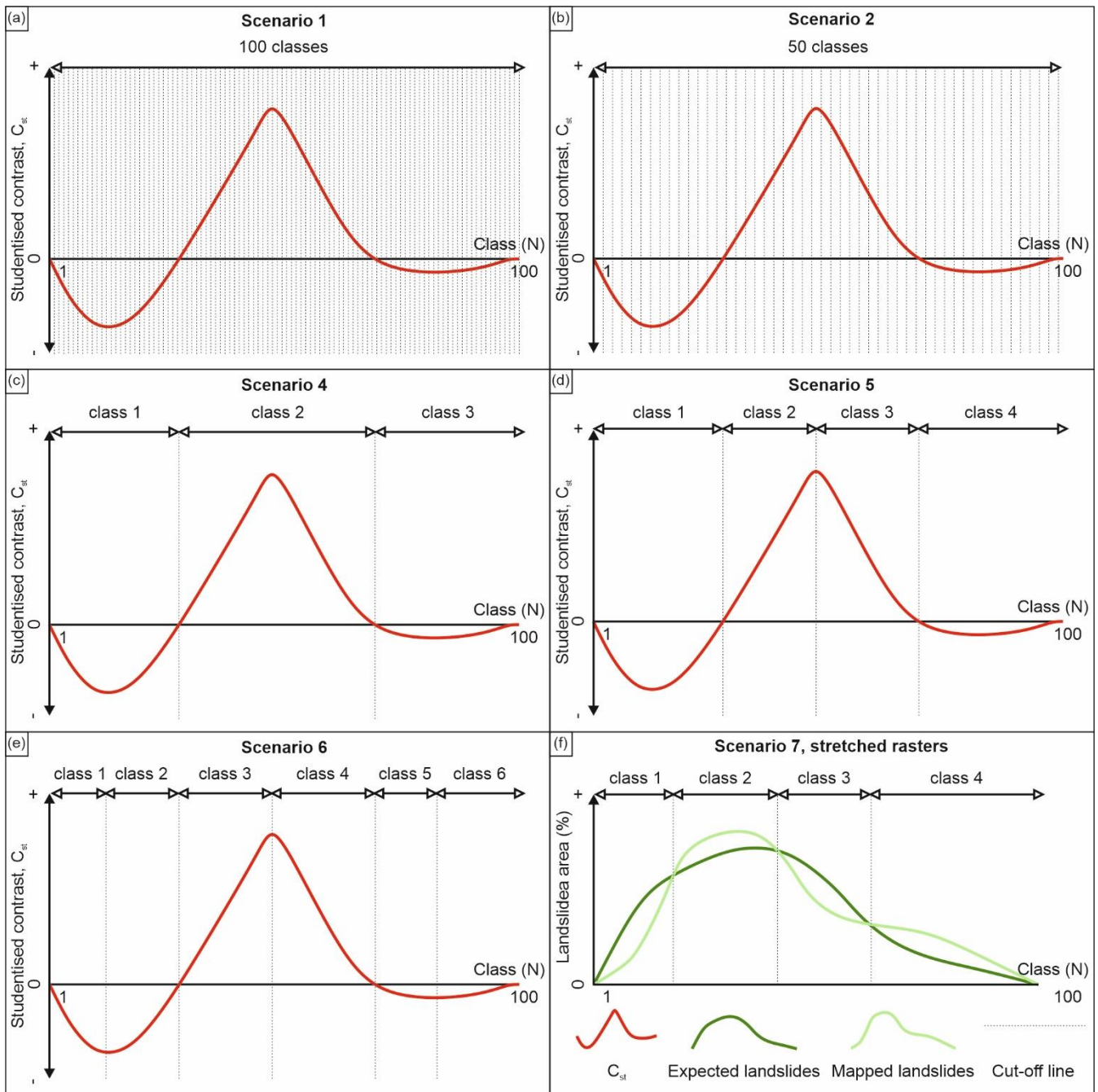
Figure 2 Theoretical example of the studentized contrast and landslide density curves for the methodology applied to define cut-off values in scenarios S1 (a), S2 (b), S4 (c), S5 (d), S6 (e) and S7 (f), respectively

Similarly, scenario S6 was defined with an additional cut-off line from scenario S5 at the lowest peak point of negative segments (Fig. 2e). For the theoretical example in Fig. 2c, d , e, the LCF for scenarios S4, S5 and S6 would result in 3, 4, and 6 classes, respectively.

210   For scenario S7, the amount of expected and mapped landslide pixels was determined for each of the 100 classes previously defined in scenario S1. For stretched rasters (e.g. elevation and slope), expected landslides are defined by the hypothesis stating that in each of 100 LCF classes the landslide density should be equal to the total study area landslide density, whereas the mapped landslide area was acquired by simple observation. After calculating the mapped and expected landslide area for each class, landslide density curves considering each class are constructed (Fig. 2f). Furthermore, the cut-off lines were determined

215   by trend changes of landslide area presence, i.e. at the points where expected or mapped landslides change to being higher or lower than the other.

For an example given in Fig. 2f, the trends change three times resulting in 3 cut-off lines, i.e. four classes. On the other hand, the constant expected amount of landslides A_{exp} for line vector LCFs used in scenario S7 was defined by:

$$A_{exp} = \frac{i}{i_{max}} \times A_{tot} \qquad (4)$$

220   where i is the buffer interval size, i_{max} the maximum reached buffer distance, and A_{tot} total landslide area. The equation aims to define an equal expected landslide area in each buffer ring. Then, the area of mapped landslides in each buffer ring is compared to the constant A_{exp}. Similarly, as with stretched rasters, trends in relations between mapped landslides being lower or higher than the constant A_{exp} define the cut-off lines. It should be noted that a training landslide dataset was used for calculations needed to define scenarios S4-S7.

225

Continuous stretched rasters and scenario S1 vector lines were reclassified using Natural Breaks (NB), Quantile (Q), and Geometrical Interval (GI) classification criteria. As a result, scenarios S8, S9 and S10 are developed, with each having ten classes, defined by NB, Q and GI reclassification criteria, respectively. Lastly, scenario S11 was defined by using stretched continuous rasters without classifying them, i.e. as input data layers containing edge values rather than classes. Moreover, the

230   aspect input data layer was applied with its original stretched values (i.e. 0-360°) representing a continuous LCF, unlike being categorical in the remaining ten scenarios. Lastly, scenario S1 line continuous LCFs with 100 equal classes were used in scenario S11 to simulate an input data layer as closely as possible. The presented classification criteria for 11 scenarios was applied uniformly, meaning each stretched raster and/or line vector was processed equally inside each scenario, yet methodologically different from other scenarios. Scenarios for proposed LCF classification criteria varies from stretched (i.e.

235   S11), partially stretched (i.e. S1 and S2), heuristic (i.e. S3), classified based on studentized contrast curve (i.e. S4, S5 and S6), classified based on expected and mapped landslide presence (i.e. S7), and lastly the commonly used classification criteria such as NB, Q and GI (i.e. S8, S9 and S10). The main aim is to test the stated classification criteria' relevance and determine its influence and necessity while using different statistical methods in a large scale case study.

3.2 Susceptibility analyses

240 Figure 3 synthesizes the methodology applied in this study that can be split into 'preparing input data', 'modeling', and 'quantitative and qualitative analyses' steps. Namely, relevant landslide and thematic (input data layers) information were obtained as described in the previous Sect. 2. Preparing input data involves deriving continuous LCF sets applicable in 11 classification scenarios and defining a fixed landslide dataset. Susceptibility analyses includes deriving 54 LSMs using the selected mapping unit with five statistical methods applied with the 11 classified factors scenarios. The quantitative and

245 qualitative analyses considered three directions: (i) model evaluation parameters, (ii) LSM validation parameters, and (iii) LSM classification parameters. Commonly used quantitative parameters are examined in all three directions, whereas the qualitative approach is made only for the LSM classification, focusing on the LSM applicability, i.e. observing spatial distribution of susceptibility classes and variability of susceptibility values. The described workflow ensures the development of landslide susceptibility maps of high quality rank according to the SQL (Guzzetti et al., 2006a,b). Lastly, the quantitative

250 and qualitative analysis results were summarized, enabling drawing the conclusions.

Preparing input data begins with splitting the polygon-based landslide inventory map randomly into two sets, each containing the same amount of polygons. Unstable training polygons (first set) were transformed into pixels, i.e. 5 m raster chosen as appropriate for LSA on a large scale done in this study. Unstable training pixels were subtracted from the study area extent, and then an equal amount of stable pixels were randomly selected in the remaining territory. This ensured an unbiased landslide

255 training set with an equal amount of stable and unstable pixels for deriving LSMs, which also defines the model training dataset for model evaluation parameters. An unstable set of polygons used for validation (second set) and all unstable polygons used for classification were transformed into 5 m rasters and used for determining LSM validation and classification parameters, respectively.

As a first step in susceptibility analyses (modeling), LCF collinearity testing was performed individually for 11 scenarios in

260 LAND-SUITE (Rossi et al., 2022). Correlations were examined by detecting LCF collinearity regarding Pearsons' R absolute value of 0.5 as the cut-off threshold. Namely, values higher than 0.5 indicate collinearity between two examined LCFs, suggesting excluding one from the further susceptibility analyses. Selected LCFs showed no collinearity in all 11 scenarios. Furthermore, 54 LSMs were derived using the prepared landslide dataset and 11 LCF sets in the five selected methods, i.e. Information Value (IV), Logistic Regression (LR), Neural Network (NN), Random Forests (RF) and Support Vector Machine

265 (SVM). It should be noted that the IV method was not applied in scenario S11, as described further below. The methods' optimization is out of the scope of this study, as they are already widely known, and their usage is discussed by researchers in LSA studies. For a detailed theoretical background about the methods applied in this paper, the readers should read van Westen, (1993) and Merghadi et al., (2020).
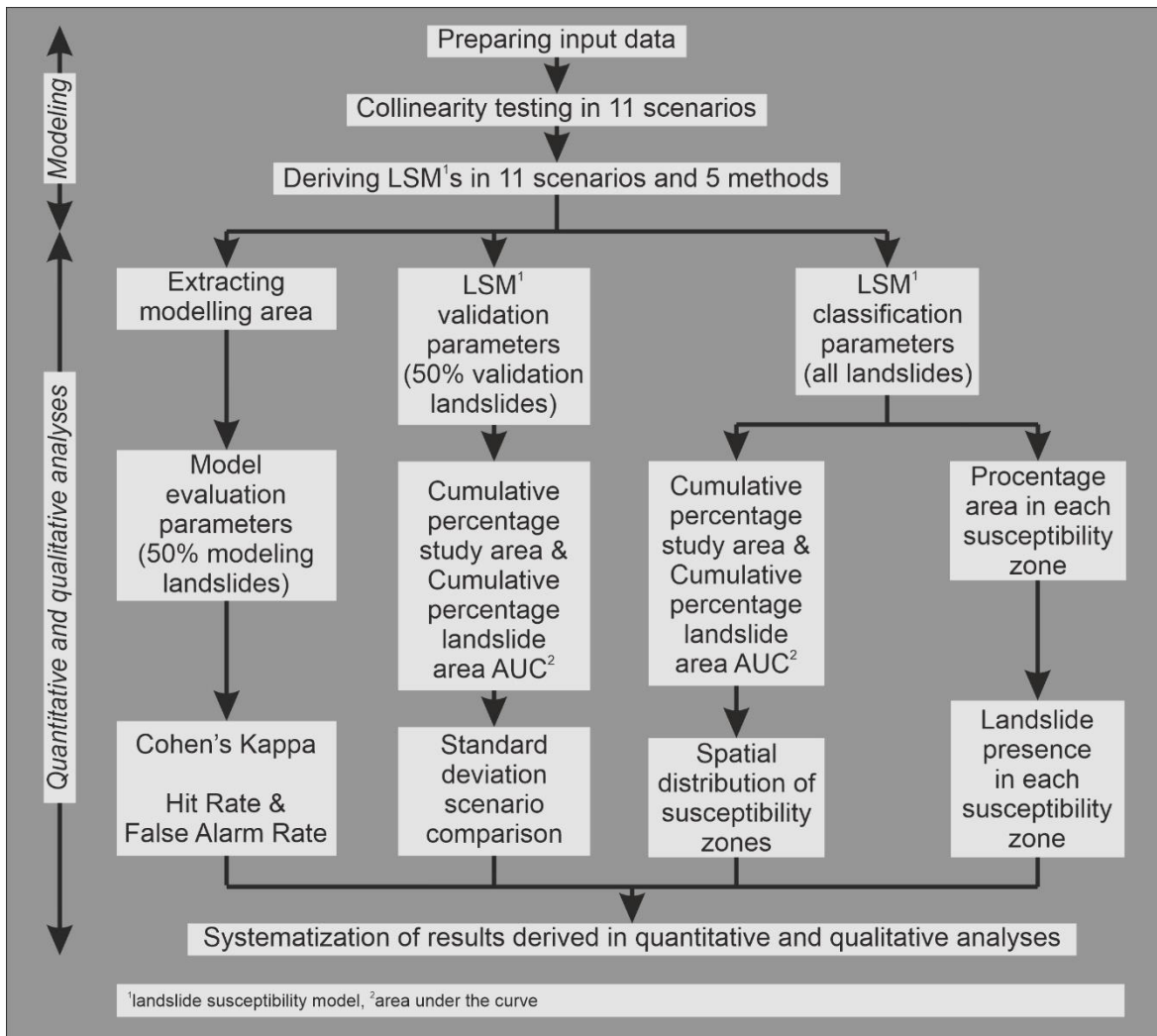
270   **Figure 3 Landslide susceptibility modelling workflow**

IV is a simple bivariate statistical method developed by Yin and Yan, (1988). Based on landslide density, using the equation:

$$I_i = log\frac{S_iN}{N_iS} \tag{5}$$

where S_i is the amount of landslide pixels in the observed class; N_i the number of pixels in the observed class; S the number
275   of landslide pixels used for model training; N amount of pixels in the study area and I_i the information value of the observed
variable. Positive and negative I_i values indicate instability and stability, respectively, whereas higher values indicate a
stronger relationship. Detailed methodology for using the bivariate statistical approach in landslide susceptibility analyses is
given in van Westen, (2002), whereas IV is applied by Sarkar et al., (2013), Farooq and Akram, (2021) and Krkač et al., (2023)
in different LSA.

280   To achieve posterior probability, i.e. probabilistic [0,1] susceptibility values, the numerical I_i is converted using the equation:

$$y = \frac{e^{f(x)}}{1+e^{f(x)}} \tag{6}$$

where: $f(x)$ is the numerical susceptibility value (input) and y the probabilistic susceptibility value (output) as defined by Bonham-Carter, (1994). The described equation has a 0.5 cut-off value, defining <0.5 and >0.5 values as stable and unstable, respectively.

285   IV is the only method in this study using only unstable modelling pixels for training, whereas other methods also require the randomly generated stable pixels. Consequently, IV LSM is not derived for scenario S11 as IV only applies to LCFs with classes, i.e., not compatible with continuous stretched input data layers that define scenario S11. On the other hand, scenario S1 with 100 equal classes approximates scenario S11 and can be considered as the closest alternative.

    Introduced with the early work of Cox, (1958), LR today corresponds to the most common statistical classification method
290   used in LSA (Reichenbach et al., 2018), as seen in the study cases from Rossi et al., (2010), Hemasinghe et al., (2018), and Bornaetxea et al., (2018), with practical code in a software application is available in LAND-SUITE (Rossi et al., 2022). A linear fitting function (Z) between landslides for n amount of conditioning variables is defined with the equation:

$$Z = b_0 + b_1X_1 + b_2X_2 + \cdots + b_nX_n \tag{7}$$

where: b_0 is the intercept of the model, b_n the partial regression coefficients, and X_n is the conditioning variable. Lastly, a
295   common application of the LR method includes converting resulting Z values to probabilistic output by applying equation [6] as mentioned in Bornaetxea et al., (2018) and Merghadi et al., (2020).

    NN is a two-stage regression or classification model that can handle multiple quantitative responses (Hastie et al., 2009). Among artificial NN methods, in this study feedforwarding was applied, indicating the flow of information exclusively in one direction. NN models are generally composed of simple circuits of nodes connected to each other (Merghadi et al., 2020),
300   defined with three layers, i.e. input layer, hidden layer and output layer. The structure applied in this paper is as follows: input layer, first fully connected layer, rectified linear unit activation function, final fully connected layer, softmax function and output. The softmax function which was applied to the final fully connected layer is defined as:

$$f(x_i) = \frac{e^{(x_i)}}{\sum_{j=1}^{K} e^{(x_j)}} \tag{8}$$

where: K is the amount of classes of response variables in the final fully connected layer and x_i each input, resulting in
305   probabilistic [0,1] values, i.e. $f(x_i)$. Merghadi et al., (2020) summarize NN as a "black box" method, unable to interpret relations between input and out variables. However, the method is popular in LSA (Reichenbach et al., 2018), with Habumugisha et al., (2022) even testing different settings to develop a method comparison, such as convolutional, deep and recurrent NN models. Furthermore, the successful applicability of different NN variations is found in the work of Lee, (2006), Nefeslioglu et al., (2007), Pascale et al., (2013), as well as in the LAND-SUITE software (Rossi et al., 2022).

310   Introducing the concept of bagging and random feature selection by Ho, (1995) and Breiman, (2001), RF are based on decision trees and provides an improvement over bagged trees (James et al., 2013). Bagging is a procedure introduced to reduce the

variance of statistical learning methods, particularly useful for decision trees (James et al., 2013). Defining p as the number of total predictors, and m as the number of predictors taken at each split, in bagging, decision trees are built using the expression:

$$m = p \tag{9}$$

315 compared to RF, where the relation is defined as:

$$m = \sqrt{p} \tag{10}$$

Namely, the algorithm does not consider most predictors in each decision tree in the RF method. As a result, RF tends to produce precise results and has an increasing popularity in LSA from 2010 onward (Merghadi et al., 2020), as depicted in several papers such as Catani et al., (2013), Wang et al., (2021), Sandić et al., (2023). Moreover, ensemble methods, including

320 RF, are remarked with excellent performance by Merghadi et al., (2020).

SVM is introduced by Cortes and Vapnik, (1995) and Vapnik, (1995), whereas James et al., (2013) describe SVM as an extension of a support vector classifier that can convert a linear classifier into one that automatically produces non-linear boundaries. Moreover, SVM can deal with linearly separable data and linearly non-separable data, whereas points that constrain the width of the margin, i.e. are closest to the optimal hyperplane, are called support vectors. To better classify most

325 training observations, the support vector classifier allows for a certain amount of observations on the wrong side of the hyperplane or the margin (James et al., 2013). The SVM uses kernel functions to transform originally non-separable data from two-dimensional into three-dimensional feature space (Ballabio and Sterlacchini, 2012), where the optimal hyperplane is constructed, and later used to classify new data. Binary classification applied in this study, i.e. 0 being stable and one unstable pixels results in better prediction efficiency than a one-class SVM application (Yao et al., 2008). Also, equation [6] is applied

330 to convert numerical susceptibility values to probabilistic ranging [0,1]. Merghadi et al., (2020) identified SVM starting a continuous increase in usage in landslide susceptibility studies since 2010 (e.g. Yao et al., 2008, Pradhan, 2013, Kavzoglu et al., 2014) and characterized SVM as having above average performance with moderately easy implementation.

3.3 Quantitative and Qualitative analysis

A landslide training set containing unstable and stable modelling pixels was examined to determine model evaluation

335 parameters, i.e. fitting performance by determining Cohen's kappa and AUC for False Alarm Rate and Hit Rate metrics. Cohen's kappa and AUC are often used statistical parameters in landslide susceptibility analyses to evaluate the model, e.g. Pourghasemi et al., (2021) and Tyagi et al., (2023). Concretely, Cohen's Kappa value interpretation was defined in Landis and Koch, (1977) as: (i) almost perfect $(0.8 - 1)$, (ii) substantial $0.61 - 0.8)$, (iii) moderate $(0.41 - 0.60)$, (iv) fair $(0.21 - 0.40)$, (v) slight $(0.00 - 0.20)$ or (vi) poor (<0.00), and the equation to determine the metric is:

340 $$\text{Cohen's Kappa} = \frac{2 \times (TP \times TN - (FN \times FP)}{(TP + FP) \times (FP + TN) + (TP + FN) \times (FN + TN)} \tag{11}$$

Where TP are true positives (i.e. landslide pixels classified as unstable), FN are false negatives (i.e. landslide pixels classified as stable), TN are true negatives (i.e. non-landslide pixels classified as stable), and FP are false positives (i.e. non-landslide pixels classified as unstable) (Gorsevski et al., 2006).

In this study, the susceptibility values were split into 100 classes with 0.01 susceptibility intervals, i.e. defining the classification thresholds used for AUC calculation. TP, FN, TN and FP pixels were determined using 0.5 as a probabilistic susceptibility cut-off value for each interval. Moreover, when the ROC curve was defined, the AUC was calculated to further estimate model fitting performance as in Rossi et al., (2010), Bornaetxea et al., (2018), Wang et al., (2021), whereas the Hit Rate and False Alarm Rate values were defined by Fawcett, (2006) as:

$$\text{Hit Rate} = \frac{\text{TP}}{\text{TP+FN}} \qquad\qquad (12)$$

and

$$\text{False Alarm Rate} = \frac{\text{FP}}{\text{FP+TN}} \qquad\qquad (13)$$

AUC values closer to 1 indicate a perfect prediction, contrary to 0.5 value corresponding to random prediction. An example for describing performance given by the AUC values is as follows: (i) <0.7 poor; (ii) 0.7-0.8 fair; (iii) 0.8-0.9 good and (iv) >0.9 excellent (Fressard et al., 2014).

Unstable validation pixels are used to derive a Cumulative percentage study area and Cumulative percentage landslide area, defining prediction performance as introduced by Chung and Fabri, (1999) and Chung and Fabri, (2003). The metric is often used in bivariate LSA approach (e.g. van Westen et al., 2003, Sinčić et al., 2022b, Bernat Gazibara et al., 2023) and is defined as success rate and prediction rate for fitting and predictive performance, respectively.

The standard deviation (SD) maps for susceptibility values are implemented to measure each scenario's stability and method's stability, resulting in qualitatively detecting uncertainty zones. Namely, 11 SD maps are developed for each of the 11 scenarios by observing the five applied methods in each scenario, i.e. to measure deviations among the methods. Furthermore, five SD maps describing criteria are defined by observing 11 scenarios applied for each method, i.e. to measure deviations among scenarios. Considering the probabilistic result of each LSM from 0.0 to 1.0, SD classes are determined with 0.1 threshold intervals to observe their presence and spatial distribution in the study area. Qualitatively, all classified SD maps are presented to illustrate spatial distribution, which is also measured quantitatively by determining the percentage area of each SD class in every derived map.

By observing all unstable pixels, AUC values were determined for the Cumulative percentage study area and Cumulative percentage landslide area curve. The latter presents AUC for LSM classification, whereas all unstable pixels are the sum of unstable pixels used for fitting performance (model evaluation) and predictive performance (validation).

Observing both stable and unstable pixels for model evaluation by Cohen's kappa and False Alarm Rate and Hit Rate AUC metrics were chosen due to their equal presence in the model training. On the other hand, measuring only unstable pixels for validation and classification by developing a Cumulative percentage study are and Cumulative percentage landslide area curve was selected to emphasize landslide occurrence exclusively for validation and classification without considering stable pixels. It should be noted that all AUC values presented in this paper, i.e. fitting, predictive, and classification performance, are expressed in rates, meaning 100 and 50 correlate to 1.0 and 0.5, respectively.

For uniform comparison, LSMs were classified in this paper according to probabilistic susceptibility values by using cut-off values from Bornaetxea et al., 2018, resulting in five susceptibility zones: (i) very low (0.0 – 0.2), (ii) low (0.2 – 0.45), (iii) medium (0.45 – 0.55), (iv) high (0.55 – 0.8), (v) very high (0.8 – 1.0). Quantitatively, for every 54 LSMs, the class area size is observed, including landslide presence in each class. Furthermore, classified LSMs are qualitatively illustrated with training 380 and validation landslides to observe spatial distribution, including close up views by overlapping them on high-resolution hillshade maps to investigate spatial accuracy, robustness, and pixelization degree.

4 Results

4.1 Landslide conditioning factors

In this section, differences between the 11 scenarios described for classifying continuous LCFs are explained on elevation LCF
385   map, quantitatively (Table 4, Fig. 4) and qualitatively (Fig. 5). Moreover, a general overview of all LCFs with the number of classes through 11 scenarios is presented in Table 3, as well as class area distribution in Fig. 7. Following the described methodology, all LCFs in S1 and S2 scenarios keep a rather stable number of classes at a 90-101 and 46-51 range, respectively. The shortage of classes in slope and terrain wetness LCFs is due to missing certain values in the original stretched raster. As intended, with a fixed amount of 10 classes, S8 to S10 scenarios have identical amounts of classes for all LCFs. Regarding the
390   heuristic S3 scenario, the number of classes varies from 7 classes at elevation to 13 classes in proximity to faults. A relatively low number of classes are depicted in S4 to S6 scenarios where continuous rasters have 2 to 6 classes, whereas vector line (buffer) LCFs show a larger span from 2 to 25 classes. Namely, proximity to geological contact has significantly more classes than other LCFs, followed by proximity to streams and faults. An exception is proximity to drainage network LCF, having 2 to 4 classes in S4-S6 scenarios. As intended, the number of classes in each LCF increases from scenario S4 to scenario S6.
395   The S7 scenario has the lowest number of classes in all LCFs, the highest number of classes being four at proximity to geological contact and the lowest two classes in proximity to drainage network, streams and faults LCF. Edge raster values and edge buffer values defined for the S11 scenario representing input data layers files are depicted in Table 3.

Table 3 Amount of class number (or values) distribution for seven continuous LCFs in 11 scenarios

		Amount of classes in a continuous LCF (N)						
		Elevation	Slope	Terrain wetness	Prox. to streams	Prox. to drainage network	Prox. to geological contact	Prox. to fault
S1		100	91	90	101	100	99	99
S2		50	46	46	51	50	50	50
S3		7	10	12	12	8	12	13
S4		3	2	3	8	2	13	6
S5		4	3	3	11	3	20	9
S6		6	4	4	14	4	25	12
S7		3	3	3	2	2	4	2
S8		10	10	10	10	10	10	10
S9		10	10	10	10	10	10	10
S10		10	10	10	10	10	10	10
		Edge raster values			Edge buffer values (m)			
S11	FROM	122.15	0.71	2.14	12	1.7	12.5	13
	TO	439.94	80.26	19.90	1212	170	1237.5	1287

400

To obtain 100 classes for the S1 scenario and 50 classes for the S2 scenario, equal interval values in the elevation LCF are 3.2 m a.s.l., and 6.4 m a.s.l, respectively. Furthermore, the heuristic interval for the scenario S3 is chosen at 50 m a.s.l. Scenarios S4 to S6 are defined with C_{st} curves based on scenario S1 classes, as illustrated in Fig. 4. For elevation LCF, the curve is defined with two negative segments in which C_{st} values reach roughly –9 and –7 minimum values, respectively. The

405 positive segment has a steep increase at class 12, leading to a C_{st} value of 16 at class 24, followed by a decrease in value reaching 0 in class 41, followed by below 0 values. Lastly, class 63 and higher have a C_{st} value of 0, indicating no landslide presence. Figure 4 illustrates that when defining scenario S7, the relation in expected and mapped landslides changes twice, defining three classes. Namely, there are more expected landslides in classes 1 to 13 and 41 to 63, whereas from 13 to 41 there are more mapped than expected landslides. Regardless of having an equal number of classes, the reclassification cut-off values

410 significantly differ for scenarios S8, S9, and S10, as depicted in the example on elevation (Table 4). On the other hand, despite having a different methodology, scenarios S4 and S7 show minimal differences in the cut-off values for the elevation LCF.

Table 4 Elevation reclassification cut-off values distribution in 10 scenarios

Class (N)	Elevation (119.0 – 436.9 m a.s.l.) reclassification cut-off values									
	S1	S2	S3	S4	S5	S6	S7	S8	S9	S10
1	122.2	125.3	150.0	153.9	153.9	138.1	157.1	152.5	150.0	148.9
2	125.3	131.7	200.0	249.3	179.4	153.9	246.2	178.6	167.4	171.1
3	128.5	138.1	250.0	436.9	249.3	192.1	436.9	202.2	183.6	187.6
4	131.7	144.4	300.0	-	436.9	249.3	-	224.5	198.5	199.7
5	134.9	150.8	350.0		-	274.8		245.7	213.4	216.2
6	138.1	157.1	400.0			436.9		266.8	229.5	238.4
7	141.2	163.5	>400			-		290.4	145.7	268.3
8	144.4	169.8	-					316.5	261.8	308.8
9	147.6	176.2						351.2	287.9	363.3
10	150.8	182.6						436.9	436.9	436.9
11	153.9	188.9						-	-	-
…	…	…								
49	274.8	430.6								
50	278.0	436.9								
51	281.1	-								
…	…									
99	433.8									
100	436.9									

415

Figure 4 Elevation landslide conditioning factor class cut-off values determined for scenarios S1 (a), S2 (b), S4 (c), S5 (d) and S6 (e) based on studentized curve, and for scenario S7 (f) based on landslide density curve

Considering class area distribution illustrated in Fig. 5 for the elevation LCF map, scenarios S1 and S11 (Fig. 5a, k, respectively) visually show little difference as intended, S1 being a simulation, i.e. approximation of S11, depicting a continuous change from low to high altitudes. With 50 instead of 100 classes, the S2 scenario depicts a somewhat rougher transition through altitude classes (Fig. 5b). Starting at three classes in scenario S4 (Fig. 5d), the second class defined with a positive C_{st} curve trend splits into two, making up four classes in the S5 scenario (Fig. 5e).
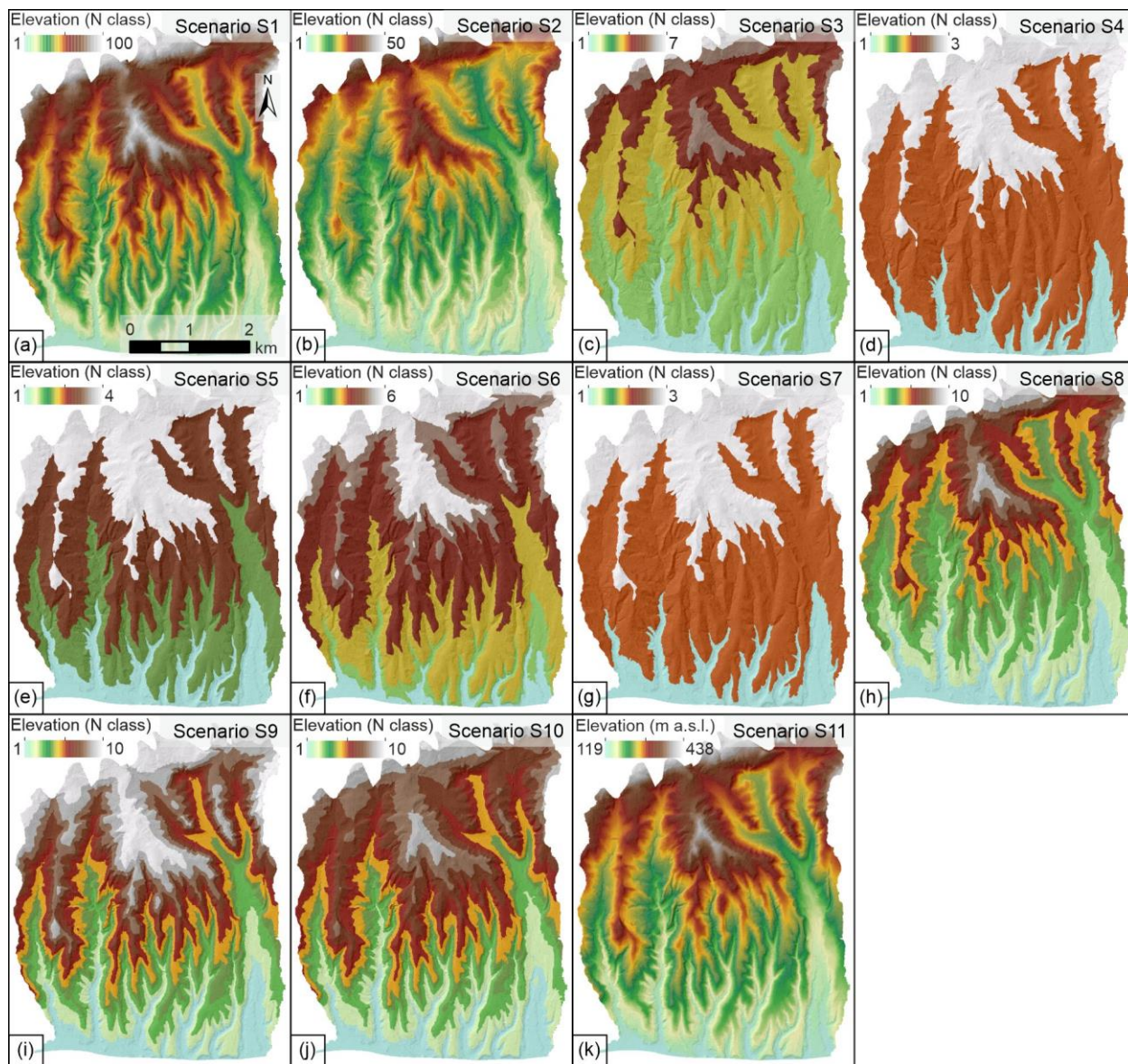
Figure 5 Maps of spatial distribution of elevation landslide conditioning factor classes for 11 scenarios

Finally, two classes defined with negative C_{st} curve trends split individually into two additional making up a final count of 6 classes for the S6 scenario (Fig. 5f). The S7 scenario is visually identical to S4 due to almost identical cut-off values depicted in Table 3. Scenarios S8, S9, and S10 (Fig. 5h, i, j) visually represent moderate differences, mainly visible in the areas of highest altitudes, i.e. the northernmost and central parts of the study area defined with classes 9 and 10. The latter classes are predominantly expressed and prevail in scenario S9 compared to scenarios S8 and S10.

Due to significant class number differences, scenarios S1 and S2 have drastically less class area size than other scenarios (Fig. 6) in all applied LCFs. Concretely, in these two scenarios, the maximum class area is found to be around 10% in proximity to geological contact, proximity to drainage network and terrain wetness LCFs. On the contrary, in the elevation LCF, the class area size does not exceed more than 5% in any class. After roughly the 30th class in scenario S2, the class area size does not exceed more than 1%. Similarly, in scenario S1, the classes in the interval from 60 to 100 usually have nearly 0% class area size. In scenarios S1 and S2, elevation, slope, proximity to all streams and terrain wetness LCFs have an increasing trend in class area size, reaching a maximum followed by a decreased trend. Proximity to geological contact, proximity to fault and proximity to drainage network show only a decreasing trend in scenarios S1 and S2, an exception being proximity to drainage network in scenario S1 with a short exchange of increasing and decreasing trends. For scenarios S3 to S10, all LCFs have around 10 to 14 classes, except proximity to geological contact, which has 24 classes. In any case, for all LCFs in scenarios S3 to S7, most area is contained in the first few classes, e.g. up to class 3 or 4. In elevation, slope and proximity to geological contact LCFs, the maximum class area size is roughly 60%, compared to roughly 80% class area size in terrain wetness, proximity to faults, drainage network and all streams LCFs. Generally, in scenarios S3 to S7 the class area size tends to drastically change from class to class, unlike scenarios S8 to S10, which depict slight changes. As methodologically defined, scenario S9 contains the 10% class area trend through all scenarios, whereas scenario S9 has significantly less class area size in classes 7 to 10, compared to classes 1 to 6.

450
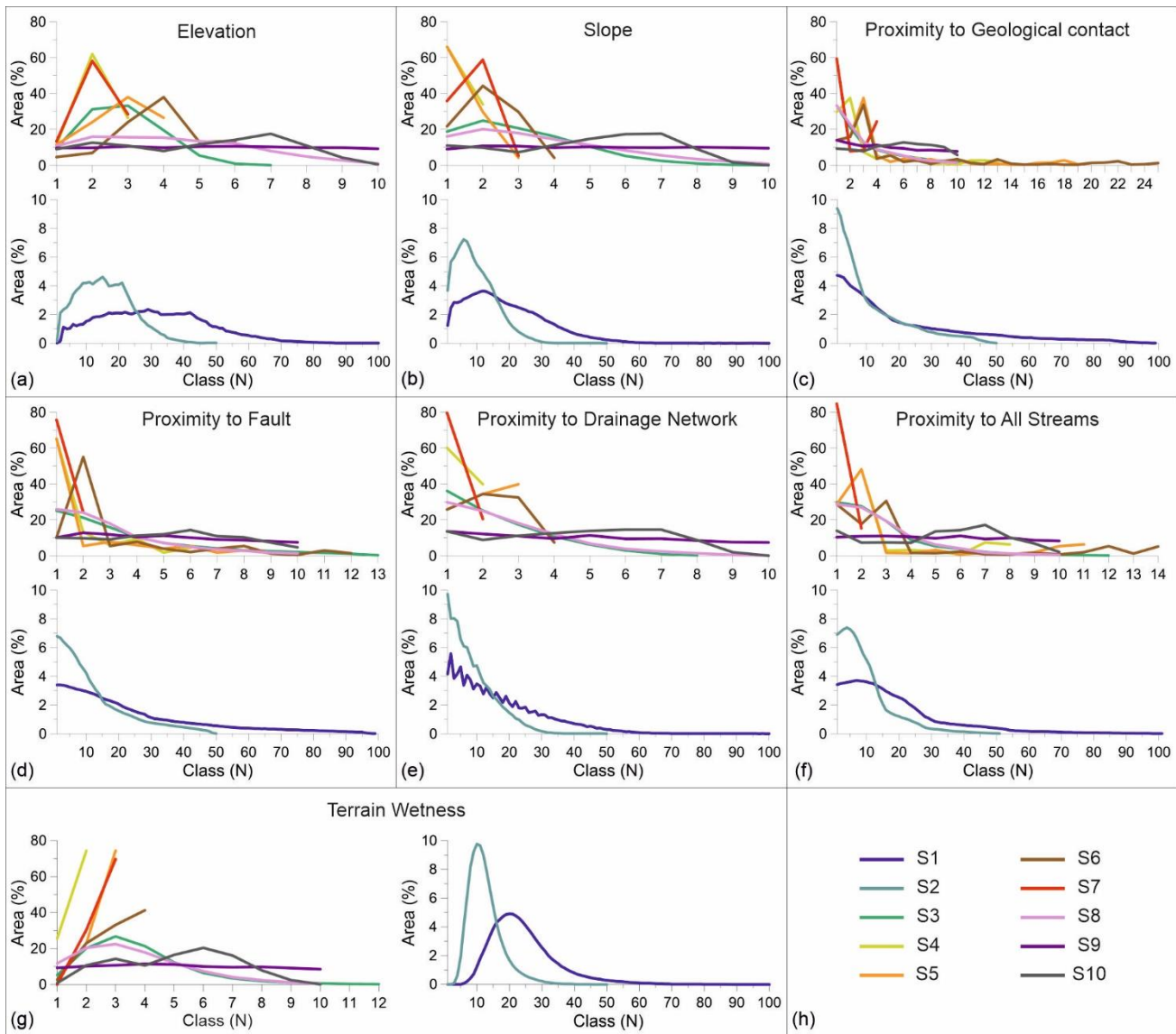
Figure 6 Graphs of class area distribution for continuous landslide conditioning factors in scenarios S1 to S10

4.2 Landslide susceptibility model evaluation

Model evaluation parameters consider both stable and unstable pixels used for training the model and expose their fitting
performance as illustrated in Fig. 7. Namely, Cohen's kappa index has a substantial agreement in all 11 scenarios for IV, LR,
NN, and SVM methods, ranging roughly from 0.6 to 0.7. The latter methods follow the same trend in all scenarios, with NN
showing the best performance (0.7), followed by LR (0.65), and finally, SVM and IV (0.6). RF method showed perfect
agreement with 1.0 or near 1.0 values in S1, S2, S3, S6, S8, S9, S10, and S11 scenarios, and drastically lower, i.e. 0.7 in the
S7 scenario. Scenarios S4 and S5 in RF performed slightly worse but still with almost perfect agreement, having Cohen's

Kappa values 0.88 to 0.96, respectively. Regarding False Alarm Rate and Hit Rate AUC values, the RF method follows the behavior of Cohen's kappa values, having excellent performance and nearly identical trends as Cohen's kappa through 11 scenarios. IV, LR, and SVM methods depict nearly identical AUC values in all 11 scenarios, ranging from roughly 85.5 to 88.5. In scenarios S4, S5, S6, and S7, the latter methods show values closer to 85.5, whereas the IV method has somewhat poorer results in scenarios S8, S9, and S10. Having the most stable AUC values in all 11 scenarios, the NN method performed excellent with AUC values ranging from 90.5 to 92, which is moderately better than IV, LR, and SVM, yet significantly worse than perfect agreements in the RF method.
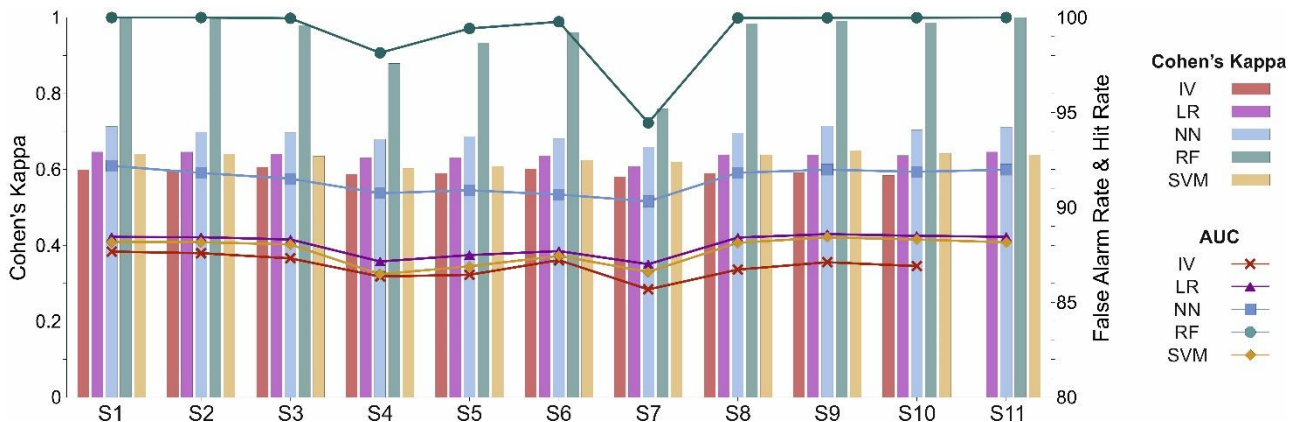
Figure 7 AUC and Cohen's Kappa quantitative parameters describing fitting performance of 54 derived landslide susceptibility models

4.3 Landslide susceptibility model validation

Unlike results in model evaluation, where studied metrics showed significant differences between five methods, by validating the LSMs, we notice lesser differences with clustered AUC values between methods (Fig. 8). Measuring the predictive performance of LSMs on an independent landslides' dataset results with scenarios S1, S2, S3, S8, S9, S10, and S11 defined with ten or more classes in LCFs as better solutions. In the latter scenarios, the AUC values range from roughly 86.5 to 88.5 for all methods, compared to a decrease in scenarios S4, S5, S6, and S7, where AUC values reach approximately 84 to 87.5. Generally, methods are similar in all scenarios and deviate minimally in scenarios S1, S2, S3, S8, S9, S10, and S11 (approx. 1.5), and moderately in scenarios S4 to S7. Concretively, S11 has proven as a scenario with minimum AUC deviations (<1) between methods, compared to the highest deviations in scenarios S4, S5, S6, and S7 (approx. 3). LR has the best prediction performance in all scenarios with the highest values reaching up to 88.5. Furthermore, LR AUC values are higher up to 3 points compared to RF, which has the least predictive performance, except in scenarios S1 and S2. Having lesser AUC values in most scenarios than LR, NN, and SVM, the IV value method nearly has the best predictive performance in the S7 scenario.

On the contrary, LR, NN, and SVM outperform IV in scenarios S8, S9, and S10. Lastly, IV, NN, and SVM have similar predictive performances in scenarios S4, S5, and S6, outperforming RF significantly.
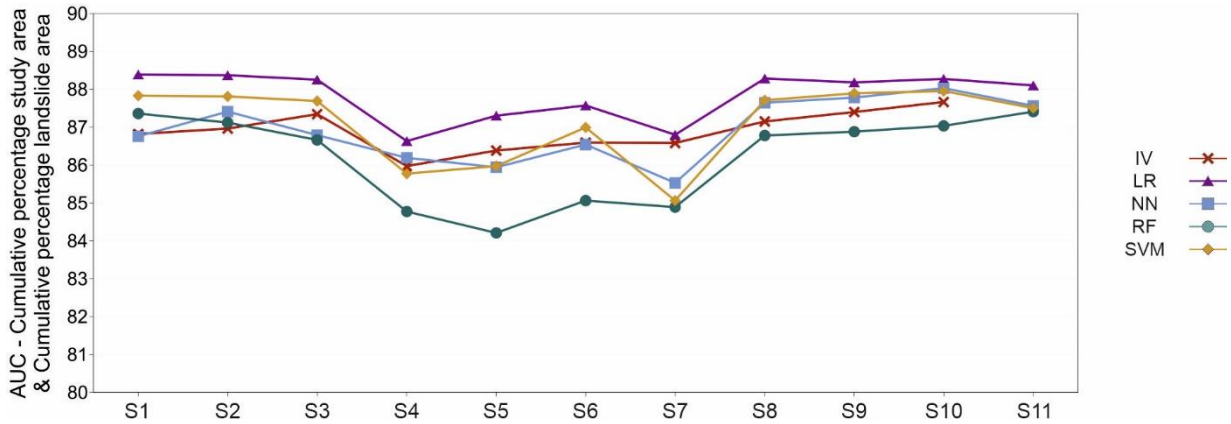
Figure 8 AUC quantitative parameter describing predictive performance of 54 derived landslide susceptibility models

4.4 Landslide susceptibility model classification

AUC classification values, measuring all unstable pixels as a combination of fitting and predictive performance, show very high values (Fig. 9). IV, LR, NN, and SVM methods show low deviations from scenario to scenario, mainly clustered with AUC values in the range of 84.5 to 89. RF method outperforms the other methods by having AUC values ranging lowest 89 in S7 up to >93 in S11 and S1. After RF, NN proved to be an alternative, having slightly higher AUC values than IV, LR, and SVM, which differentiate minimally in each observed scenario. All methods show lower AUC values in scenarios S4, S5, and S6, with a minimum in scenario S7.
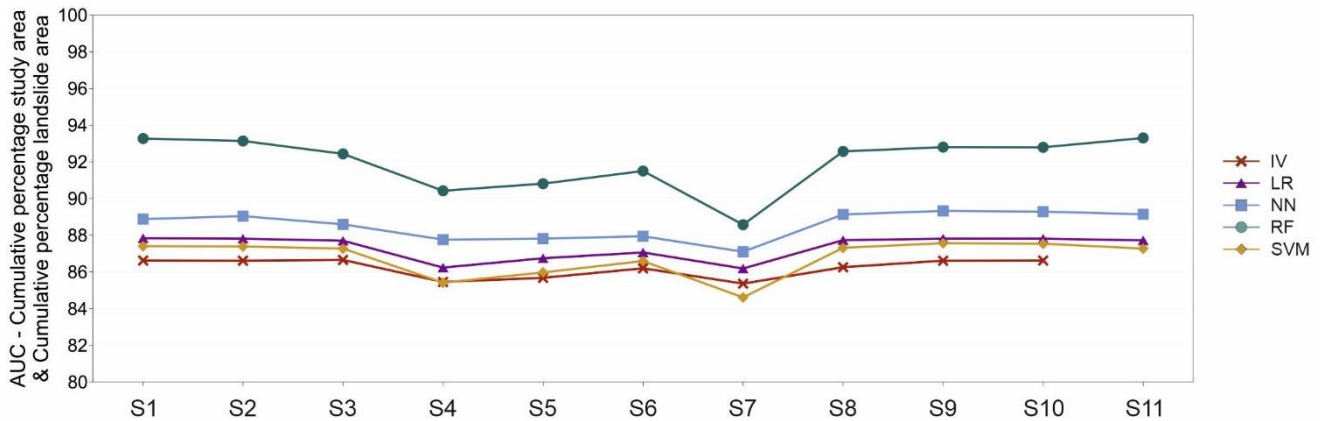
Figure 9 AUC quantitative parameter describing classification performance of 54 derived landslide susceptibility models

In scenarios S1, S2, S3, S8, S9, S10, and S11, all methods show AUC values higher than 86. Lastly, the RF method is the only method significantly influenced by the number of LCF classes, with significantly lower AUC values in scenarios S4, S5, S6, and S7.

To identify classification parameters, derived LSMs are firstly classified in zones according to probabilistic susceptibility values as follows: (i) very low (0.0 – 0.2), (ii) low (0.2 – 0.45), (iii) medium (0.45 – 0.55), (iv) high (0.55 – 0.8) and (v) very high (0.8 – 1.0). Generally observing the susceptibility zones, noticeable differences are distinguishable among methods rather than scenarios (Fig. 10). All methods show <10% class area in a very high zone, with RF, SVM, and IV often having <5%. All 54 LSMs have a medium susceptibility zone smaller than 10%, with RF having a minimum with as small as 2%. Moreover, the RF method has the smallest area in high and very high susceptibility zone. Class area percentage changes are most significant in very low and low classes, whereas very high, high, and medium classes show low differences in all methods and most scenarios. IV and SVM methods tend to have fewer differences between low and very low classes, i.e. having almost equal areas in both zones. RF has the most percentage area in the very low class, followed by NN and LRM. However, RF, NN, and LR have nearly similar class area sizes in the low class. Observing very low and low zones as one, IV, LR, NN, and SVM show a lot of similarities, unlike RF, which has exceptionally high values, reaching >85% area for the cumulative area of the two classes in most scenarios. Similarly, very high and high zones contain less than 10% of the map area in the RF method, whereas the values reach around 20% for the other methods. In other words, the most significant differences are depicted individually in the relation between very low and low zone and very high and high zone. For the latter, the RF method favors having an extremely large very low zone and an extremely small very high zone. On the contrary, IV and SVM tend to have rather large low and high zones. NN has around 10% smaller very low zone compared to RF, followed by LR with 10% smaller than NN. Lastly, IV and SVM have around 40% of the map area in the very low zone.
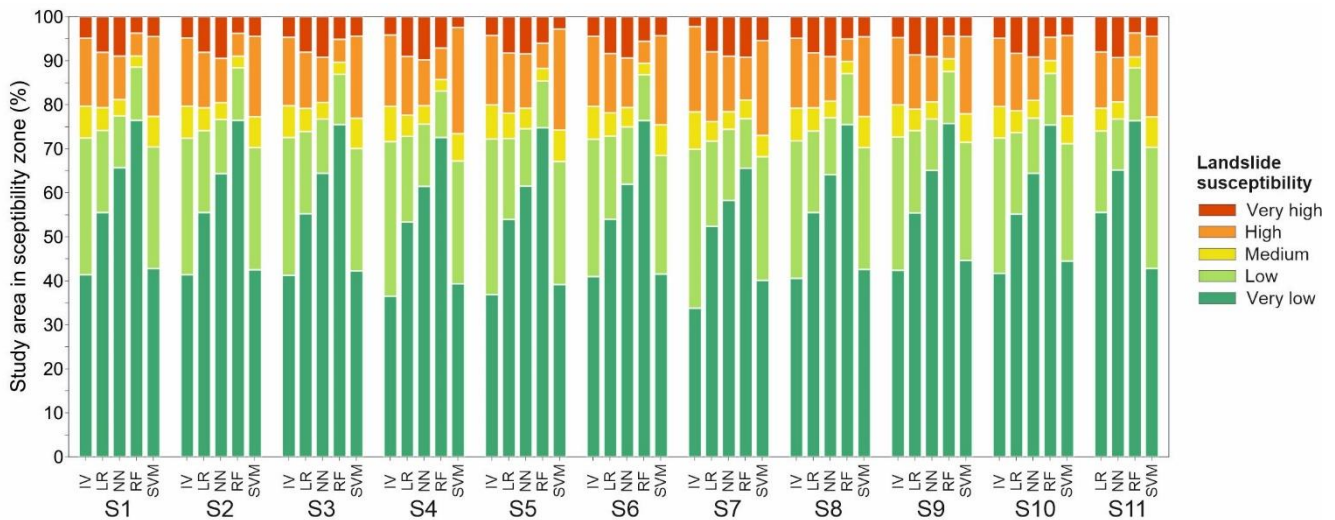
Figure 10 Landslide susceptibility zone area distribution graph for 54 derived landslide susceptibility models

The sum of landslide presence in very high and high susceptibility zone are extremely similar in all 54 LSMs (Fig. 11). However, observing the two zones individually, noticeable differences are depicted. Namely, LR, NN, and RF methods have higher landslide presence percentages in very high zone resulting in lower presence in high zone, whereas on the contrary, IV and SVM methods have less landslide presence in very high zone and higher landslide presence in the high zone. Concretely, IV and SVM have around or less than 35% landslide presence in the very high zone, compared to other methods, which often have >50%. The minimum is in the IV method scenario S7, and SVM method scenarios S4 and S5 at around 20% or less landslide presence in very high susceptibility zone. RF has the maximum landslide presence in the very high zone in each scenario, valuing on average 62%, followed by NN (approx. 56%) and LR (approx. 51%). Observing landslide presence in very low, low, and medium zones, minimal differences are noticeable, an exception being IV and SVM methods, which stand out with extremely low landslide presence in very low susceptibility zone. Moreover, the RF method has the highest amount of landslide presence in the very high susceptibility zone in each scenario and the highest landslide presence in the very low zone, reaching up to 5%. Interestingly, the average landslide presence area in the medium susceptibility zone is 5.5%, i.e. rather low.
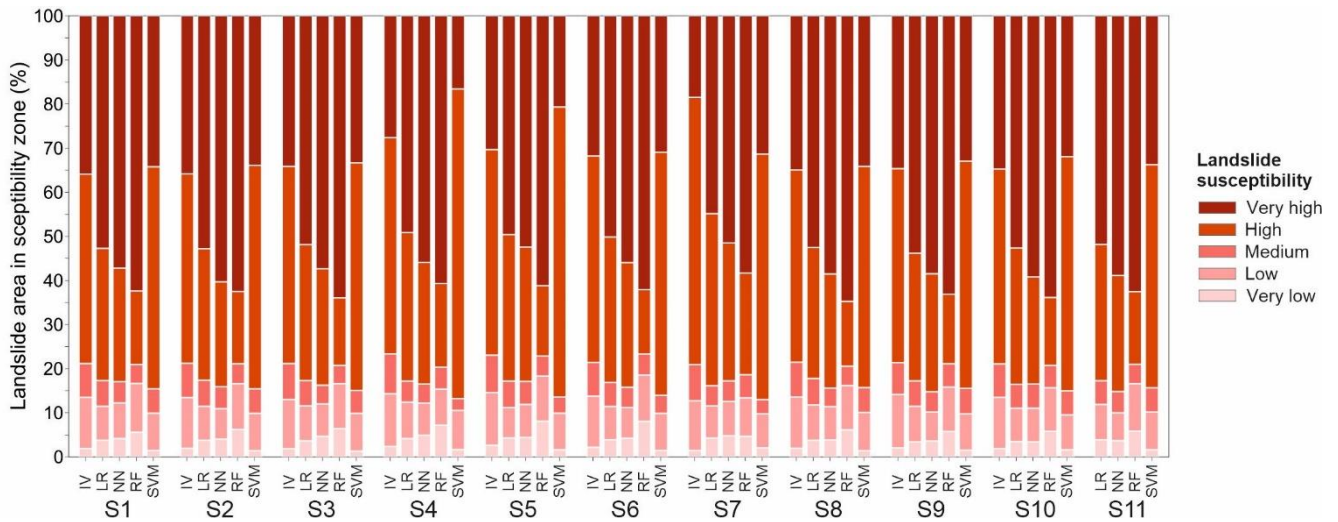
Figure 11 Landslide area distribution in landslide susceptibility zones graph for 54 derived landslide susceptibility models

5 Discussion

5.1 Discussion regarding LCF classification criteria

Considering the quantitative results in Sect. 4.2, 4.3 and 4.4 from a perspective of 11 scenarios for continuous LCFs classification, moderate differences are found in fitting performance and low in predictive and classification performance. However, the noted differences occur repeatedly in scenarios S4 to S7 and are represented by poorer performance in all studied

metrics. A likely reason behind the results is too few classes in the LCFs. Concretely, often showing extraordinary results, scenario S7 has four or fewer classes in the continuous LCFs. On the contrary, opposite classification criteria with a large number of classes, such as scenarios S1 to S3 and S8 to S10, result in satisfactory results in all scenarios and are highly similar. That implies that the closer the classification is to the continuous behavior, the LSM fitting and predictive performance is higher.

11 classified SD maps are illustrated in Fig. S1 for each LCF classification scenario, representing differences in susceptibility values between the five applied methods. Namely, classes of higher SD values, indicate higher uncertainties in the LSMs. The SD maps are visually similar, indicating low differences in susceptibility values from scenario to scenario. 0.0-0.1 SD class is most represented in all scenarios, with area presence ranging from minimum approx. 50% in scenario S5 to >65% in scenario S7. 0.1-0.2 SD class and 0.2-0.3 SD class value are equally represented in all scenarios, their area percentage being approx. 35% and 5-10%, respectively. An exception is S7, where the 0.2-0.3 SD class has less than 5%, and in S11, where the 0.1-0.2 SD class has <30% area. Qualitatively observing spatial distribution, SD class distribution does not differ significantly from scenario to scenario. An exception is scenario S11, where the 0.0-0.1 SD zone has clustered areas, unlike dispersed and likely pixelized, i.e. distributed into smaller zones as visible in other scenarios. Surprisingly, scenarios S7 and S11, which are methodologically opposite considering the number of classes, have a high >60% map area in the 0.0-0.1 SD class. Moreover, S7 stands out by having the least area in the 0.2-0.5 SD range, i.e. having >95% of the area in SD values <0.2. If they are present, 0.3-0.4 and 0.4-0.5 SD classes appear in the same locations in all scenarios. Scenario S11 stands out with the most area in the 0.3-0.4 SD class, but still <1% of the study area. Generally, the 0.3-0.5 SD range is least present and neglectable in all scenarios when compared to other classes. By observing the 11 close up views, the differences can be observed by comparing two groups, defined by the number of classes in LCFs used to derive a LSM, and scenario S7 as a standalone. Namely, the first group consists of scenarios with fewer classes in LCFs, i.e. S4, S5, and S6. Scenarios with mainly ten or more classes comprise the second group, i.e. scenarios S1, S2, S3, S8, S9, S10, and S11. The first group is less pixelized, with a low amount of standalone pixels and highly expressed susceptibility zones, unlike the second group, which has heterogeneous and pixelized small zones.

Considering the above, noticeable differences between the 11 scenarios can be traced to the number of classes present in LCFs, not to the method applied to create the classes. Consequently, scenarios S4, S5, S6, and S7 can be outlined as the less favorable ones. The latter scenarios show poorer fitting, predictive, and classification performance results. Moreover, qualitatively, they have robust susceptibility zones, i.e. loosing susceptibility information on a large scale which is essential for high spatial accuracy and applicability in spatial planning. On the other hand, robustness can ease the classification process to determine susceptibility zones, if the values related to robustness are spatially accurate. Also, compared to other scenarios, the classification process is relatively time-consuming for scenarios S4-S7. Commonly used and straightforward heuristic, NB, Q, and GI classification criteria applied in scenarios S3, S8, S9, and S10, represent satisfactory options, considering the number of classes defined. With most researchers using around ten classes in different methods, considering results from scenarios S1 and S2, a significantly larger amount of classes can also be applied to reach reliable results.

Lastly, scenario S11 can be suggested as a uniform approach to perform landslide susceptibility modelling. Scenario S11 shares excellent performance with several other scenarios, however, it stands out as the most consistent considering predictive performance with low differences between the five used methods. Similarly, it is the least pixelized in the SD map and has >60% of the map area in the 0.0 – 0.1 SD zone, proving low uncertainties between methods. Moreover, directly applying
580 stretched rasters removes a step in landslide susceptibility modelling often done by researchers, enabling more technical simplicity and reducing the time needed due to avoiding the classification of the input data layers. Considering the bivariate approach, where applying stretched rasters such as in scenario S11 without classes is not possible, we suggest scenario S1 as the closest alternative, i.e., the optimal solution.

It should be stated that the set of prepared LCFs in this study is appropriate for achieving excellent performance for deriving
585 LSMs. Moreover, the study aimed to test the 11 criteria on such a set, however, the relevance and/or importance of each LCF in the LSA was not individually determined. Hence, some of the LCFs may be of poor relation to LSA quality, and classifying them differently is irrelevant. In other words, the 11 classification scenarios would likely present more differences on a limited amount of highly important LCFs. The latter is addressed by applying the classification criteria uniformly for all continuous LCFs and proposing a uniform solution for a relevant set of LCFs, not limited only to the most significant LCFs. Similarly,
590 applying a non-representative landslide inventory map would likely cause substantial deviations to the results presented in this study. Future work considering this topic could lead to the idea presented by Yan et al., (2019), where LCFs in all scenarios are mutually combined and tested to develop an optimal solution, which would lead to a tremendous amount of LSMs in this paper and was therefore discarded, rather emphasizing in the investigations to propose a uniform approach.

5.2 Discussion regarding different statistical methods

595 Unlike low differences between the 11 scenarios, the five applied methods showed substantial deviations from each other in different quantitative and qualitative performances as seen in Sect 4.2, 4.3, 4.4. and 4.6. Namely, RF outperforms other methods significantly in model evaluation, followed by the NN method, whereas IV, LR, and SVM differ minimally and show the lowest Cohen's Kappa and AUC values. Furthermore, predictive performance favors LR, whereas RF performed poorly, leaving IV, NN, and SVM in between. Lastly, classification metrics favor RF due to perfect results in model evaluation.
600 Moreover, unlike IV and SVM, RF has the most landslide presence in a very high susceptibility zone. On the other hand, RF also excels in the area presence of a very low susceptibility zone, having it by far the largest compared to other methods while keeping a low percentage landslide presence.

Examining SD maps of susceptibility values for each method individually (Fig. S3), uncertainty through 11 scenarios is measured for each method. Surprisingly, the IV, LR, and SVM methods show minimal SD values for most of the study area.
605 Namely, the SVM method has 99% of the study area in the 0.0-0.1 SD zone, whereas IV and LR methods have <5% of the study area in the 0.1-0.2 SD zone. In addition, SVM and IV methods display noticeable uncertainty in the south, and southeastern part of the study area, whereas the LR method has them distributed through the study area. Conversely, RF and NN methods have significantly less area in the lowest SD class.

The quantitative and qualitative analysis applied to compare 54 derived LSMs showed the advantages and disadvantages of the five used methods, justifying the broader approach in this study. In model evaluation, RF often classified the training pixels perfectly, whereas the predictive performance was significantly lower, leaving an open question to investigate further. Nonetheless, a rigorous approach with an unbiased training dataset and 50 to 50 percent landslide inventory splitting still enabled high predictive performance. Moreover, RF clusters the values close to 0 and 1 susceptibility, leaving low and high susceptibility zones relatively small. However, considering landslide presence in the RF susceptibility zones, extreme landslide density in the very high zone can be observed. Interestingly, the IV method can be regarded as equally usable despite the modelling using only unstable pixels. Moreover, IV was poorly influenced by LCFs having few classes, similar to LR and SVM. All three methods showed extremely low SD values, indicating that all 11 scenarios are equally suitable for their application considering the resulting susceptibility values. On the contrary, NN and RF are affected by the lack of more classes in LCFs, i.e. should not be used recklessly. Considering the classification parameters, low landslide presence was detected in very high susceptibility zones for both IV and SVM. Despite using 100 classes for LCFs in scenario S1, SVM was the only method that had well-characterized susceptibility zones in close up views, unlike other methods, which were rather pixelized. NN, and even to a greater extent RF, seem to outperform IV, LR, and SVM considering quantitative metrics. However, the qualitative approach depicted certain drawbacks which should be noted. On the other hand, certain advantages were noted in the IV and SVM methods, despite their poorer performance. Consequently, we suggest using LR as a starting point, being the most stable with the least extraordinary results, whereas for IV, NN, RF, and SVM methods, the classification criteria can drastically influence the LSM quality, i.e. optimization should be applied as well as considering the LSA's purpose.

Considering that in many LSA comparison papers, the mentioned model evaluation and/or validation metrics reach satisfactory results in the tested scenarios, in this study, we emphasized the classification parameters because: (i) satisfactory quantitative metrics results are expected in model evaluation (fitting performance) and LSM validation (predictive performance) due to complete input data of high spatial accuracy; (ii) classification parameters take to consideration all identified unstable pixels from the complete landslide inventory; (iii) spatial distribution of classified LSMs allows insight regarding application in the spatial planning system, combined with susceptibility zone relation to elements at risk (e.g. buildings, roads); (iv) classification parameters define relations of all identified landslide presence in each defined susceptibility class, essential for application and defining landslide protocols for LSA.

Putting the differences aside, all methods resulted in objectively excellent LSMs, and confirmed the previous LSA done by Bernat Gazibara et al., (2023) in the study area. However, modelling on large scale and aiming towards application in spatial planning, using a qualitative approach has proven to be of great significance by providing new insights into landslide susceptibility modelling. Without the latter, a complete picture of the used methods would not be acquired. LSA is often carried out to optimize certain parameters (e.g. method, mapping unit, or inventory type) by developing dozens of LSMs which are further compared. When landslide susceptibility modelling reaches a point where most LSMs have a high fitting and predictive

performance, we argue that additional metrics (e.g. qualitative approach and classification parameters) are needed, depending on the scope of the LSA.

6 Conclusions

645   The presented work is based on geomorphologically significant and spatially accurate thematic data for LSMs, making it one of the rare scientific works that implements the recommendations for LSA by Reichenbach et al., (2018). More precisely, Reichenbach et al., 2018 identified that LSA researchers are more eager to experiment with modelling techniques rather than focusing on acquiring relevant thematic and landslide data. Moreover, existing literature deals with preparing thematic input data in a general way and lacks a uniform approach for continuous LCF classification. This work represents a comprehensive

650   analysis of different classification criteria for continuous LCFs and applies the most commonly used statistical methods evaluated by several quantitative and qualitative metrics to obtain representative conclusions and novelties regarding large scale LSMs.

We defined 11 classification criteria for the seven continuous LCFs applied in the landslide susceptibility modelling, namely elevation, slope, terrain wetness, proximity to geological contact, faults, streams, and drainage network. Also, two criteria were

655   applied to the categorical aspect LCF, whereas the remaining categorical LCFs, i.e. lithology (rock/type) and land use, remained constant in all scenarios. Scenarios were defined based on the classification criteria applied in the literature review and/or modifications of the criteria and vary from stretched values, partially stretched classes, heuristic approach, classification based on studentized contrast and landslide presence, and commonly used classification, such as Natural Neighbor, Quantiles and Geometrical intervals. By applying five statistical methods, i.e., IV, LR, NN, RF, and SVM, 54 LSMs were derived,

660   providing a comprehensive insight into the research issue. Also, a strict landslide sampling approach was used, with 50% of landslide polygons used for training and the other 50% for validation. Each derived LSM was measured by quantitative metrics, i.e, False Alarm Rate and Hit Rate AUC and Cohen's kappa for model evaluation, AUC prediction rate values and SD class percentage area for model validation, and AUC, susceptibility zone percentage area and landslide area presence in susceptibility zones for model classification. The complete set of studied metrics proved to be necessary, pointing out the

665   advantages and disadvantages of used methods and classification scenarios. Considering general performance, all the derived LSMs proved to be reliable considering usually studied metrics, i.e. AUC for fitting and predictive performance.

The analysis presented in the paper resulted in a set of large scale LSMs created from representative and spatially accurate input data including detailed LiDAR-based landslide inventory and high-resolution thematic data. Based on 54 reliable LSMs, specific conclusions with practical application could be made. The landslide susceptibility modelling was done on 21 km^2 in

670   the Podsljeme area, using 5 m pixel as a mapping unit suitable for large scale LSA. The study area is characterized by small and shallow landslides and can be representative of similar environments with high-quality input data for landslide susceptibility modelling. The main conclusions and novelties derived from the presented comprehensive large scale landslide susceptibility analysis are following:

(i) Due to using relevant input data with sufficient spatial accuracy, landslide susceptibility modelling performed by any statistical method or any LCF classification scenario in this paper resulted in a highly reliable LSM;

(ii) Any of the suggested scenarios to classify continuous LCFs is appropriate if it resulted in roughly ten or unlimitedly more classes in the LCF, suggesting the higher importance of the number of classes in LCFs, rather than the method of how the classes were created. In other words, a low number of classes in LCFs, such as <5, is likely to perform poorly and should be avoided;

(iii) Applying input data layers as stretched rasters (scenario S11) and line vectors as buffers with >10 buffer zones, simplifies the susceptibility modelling process and provides a uniform solution to preparing LCFs;

(iv) Quantitative classification parameters and uncertainty metrics, as well as qualitative comparison (e.g. close up views to verify spatial accuracy) applied in this study, are necessary metrics to evaluate optimal settings for large scale landslide susceptibility modeling as they depict LSM characteristics unidentified by standard quantitative fitting and/or prediction metrics;

(v) Optimal method selection remains an open question and generally should be considered regarding the final applicability of the LSA, whereas in this study LR method presents the most stable and representative option, and the RF method offers optimal performance when appropriately applied, achieving far better performance;

(vi) NN and RF methods are more sensitive to the LCF classification criteria than IV, LR, and SVM.

However, using the same strategy on a different scale or with an incomplete dataset (either irrelevant LCFs or a non-representative landslide inventory) remains an open question which requires additional research. Moreover, comprehensive comparison using a variety of parameters provides new insight into derived LSMs. For LSM validation, quantitative metrics are not representative due to the lack of a spatial accuracy component, which is especially important in large scale LSA and was proven in this paper. The studied qualitative metrics are maps of SD classes for model validation, whereas the spatial distribution of susceptibility zones and landslides in full extent and additionally with elements at risk in close up views are used to describe classified LSMs. Presented results and performed validation of LSMs contribute to the preparation of recommendations, evaluation, and use of LSMs and associated terrain zonations proposed by Reichenbach et al., (2018). The recommended qualitative metrics enable the verification of the LSMs for practical application in spatial planning at the local level because it enables comparison with real environmental conditions and elements at risk visible on close up views and high-resolution hillshade maps.

Data availability

Data supporting the research obtainable from the corresponding author upon reasonable request.

Author contribution

705 MS and SBG conceptualised the draft study design, followed by finalizing the research concept with MR. MS carried out the analyses and wrote the manuscript under SBG supervision. All authors commented and analysed the results and were included in the discussion, whereas SBG, MR, and SMA fully revised the manuscript.

Competing interests

The authors declare that they have no conflict of interest.

710 **Acknowledgements**

This research has been fully supported by the Croatian Science Foundation under the project methodology development for landslide susceptibility assessment for land use planning based on LiDAR technology, LandSlidePlan (HRZZ IP-2019-04-9900, HRZZ DOK-2020-01-2432). The work was co-funded by the Geomorphology group of the Istituto di Ricerca per la Protezione Idrogeologica, Consiglio Nazionale delle Ricerche (Perugia, Italy).

715

The authors would like to thank Paola Reichenbach for discussions and useful suggestions during the conceptualisation phase of the research.

We would like to thank the reviewers for their suggestions and comments.

720 **References**

Ballabio, C. and Sterlacchini, S.: Support Vector Machines for Landslide Susceptibility Mapping: The Staffora River Basin Case Study, Italy, Math Geosci, 44, 47–70, https://doi.org/10.1007/s11004-011-9379-9, 2012.

Bernat, S., Mihalić Arbanas, S., and Krkač, M.: Landslides triggered in the continental part of Croatia by extreme precipitation in 2013, in: Engineering geology for society and territory, volume 2: Landslide processes , 1599–1603, 2014a.

725 Bernat, S., Mihalić Arbanas, S., Krkač, M.: Inventory of precipitation triggered landslides in the winter of 2013 in Zagreb (Croatia, Europe), in: Proceedings of the 3rd World Landslide Forum, Landslide Science for a Safer Geoenvironment: Volume 2: Methods of Landslide Studies, 3rd World Landslide Forum, Beijing, China, 2-6 June 2014, 829–836, 2014b

Bernat Gazibara, S., Krkač, M., Sečanj, M., and Mihalić Arbanas, S.: Identification and Mapping of Shallow Landslides in the City of Zagreb (Croatia) Using the LiDAR–Based Terrain Model, in: Advancing Culture of Living with Landslides, Springer

730 International Publishing, Cham, 1093–1100, https://doi.org/10.1007/978-3-319-53498-5_124, 2017.

Bernat Gazibara, S., Krkač, M., and Mihalić Arbanas, S.: Verification of historical landslide inventory maps for the Podsljeme area in the City of Zagreb using LiDAR-based landslide inventory, The Mining-Geology-Petroleum Engineering Bulletin, 34, 45–58, https://doi.org/10.17794/rgn.2019.1.5, 2019a.

Bernat Gazibara, S., Krkač, M., and Mihalić Arbanas, S.: Landslide inventory mapping using LiDAR data in the City of Zagreb

735   (Croatia), J Maps, 15, 773–779, https://doi.org/10.1080/17445647.2019.1671906, 2019b.

Bernat Gazibara, S., Mihalić Arbanas, S., Sinčić, M., Krkač, M., Lukačić, H., Jagodnik, P., and Arbanas, Ž.: LandSlidePlan - Scientific research project on landslide susceptibility assessment in large scale, in: Proceedings of the 5th regional symposium on landslides in Adriatic - Balkan Region , 5th regional symposium on landslides in Adriatic – Balkan Region, Rijeka, Croatia, 23-26 March,2022, 99–106, 2022.

740   Bernat Gazibara, S., Sinčić, M., Krkač, M., Lukačić, H., and Mihalić Arbanas, S.: Landslide susceptibility assessment on a large scale in the Podsljeme area, City of Zagreb (Croatia), J Maps, 1–11, https://doi.org/10.1080/17445647.2022.2163197, 2023.

Bishop, Y. M. M., Fienberg, S. E., and Holland, P. W.: Discrete Multivariate Analysis: Theory and Practice, 1975.

Bonham-Carter, G. F., Agterberg, F. P., and Wright, D. F.: Weights of evidence modelling: a new approach to mapping mineral

745   potential, https://doi.org/10.4095/128059, 1990.

Bonham-Carter, G. F.: Geographic Information Systems for Geoscientists: Modelling with GIS, Pergamon, Ottawa, 1994.

Bornaetxea, T., Rossi, M., Marchesini, I., and Alvioli, M.: Effective surveyed area and its role in statistical landslide susceptibility assessments, Natural Hazards and Earth System Sciences, 2018.

Brabb, E. E.: Innovative Approaches to Landslide Hazard Mapping, in: Proceedings of 4th International Symposium on

750   Landslides, 307–324, 1984.

Breiman, L.: Random Forests, Mach Learn, 45, 5–32, https://doi.org/10.1023/A:1010933404324, 2001.

Catani, F., Lagomarsino, D., Segoni, S., and Tofani, V.: Landslide susceptibility estimation by random forests technique: sensitivity and scaling issues, Natural Hazards and Earth System Sciences, 13, 2815–2831, https://doi.org/10.5194/nhess-13-2815-2013, 2013.

755   Chen, W., Xie, X., Wang, J., Pradhan, B., Hong, H., Bui, D. T., Duan, Z., and Ma, J.: A comparative study of logistic model tree, random forest, and classification and regression tree models for spatial prediction of landslide susceptibility, Catena (Amst), 151, 147–160, https://doi.org/10.1016/j.catena.2016.11.032, 2017.

Chung, C. J. F. and Fabbri, A. G.: Probabilistic Prediction Models for Landslide Hazard Mapping, Photogramm Eng Remote Sensing, 65, 1389–1399, 1999.

760   Chung, C.-J. F. and Fabbri, A. G.: Validation of Spatial Prediction Models for Landslide Hazard Mapping, Natural Hazards, 30, 451–472, https://doi.org/10.1023/B:NHAZ.0000007172.62651.2b, 2003.

City of Zagreb: Land use map of City of Zagreb, 2011.

Corominas, J., van Westen, C., Frattini, P., Cascini, L., Malet, J.-P., Fotopoulou, S., Catani, F., Van Den Eeckhaut, M., Mavrouli, O., Agliardi, F., Pitilakis, K., Winter, M. G., Pastor, M., Ferlisi, S., Tofani, V., Hervás, J., and Smith, J. T.:

765   Recommendations for the quantitative analysis of landslide risk, Bulletin of Engineering Geology and the Environment, https://doi.org/10.1007/s10064-013-0538-8, 2014.

Cortes, C. and Vapnik, V.: Support-vector networks, Mach Learn, 20, 273–297, https://doi.org/10.1007/BF00994018, 1995.

Cox, D. R.: The Regression Analysis of Binary Sequences, Journal of the Royal Statistical Society, 20, 215–242, 1958.

Cui, K., Lu, D., and Li, W.: Comparison of landslide susceptibility mapping based on statistical index, certainty factors,
770   weights   of   evidence   and   evidential   belief   function   models,   Geocarto   Int,   32,   935–955, https://doi.org/10.1080/10106049.2016.1195886,   2017.

Donati, L. and Turrini, M. C.: An objective method to rank the importance of the factors predisposing to landslides with the GIS methodology: application to an area of the Apennines (Valnerina; Perugia, Italy), Eng Geol, 63, 277–289, https://doi.org/10.1016/S0013-7952(01)00087-4, 2002.

775   Dou, J., Tien Bui, D., P. Yunus, A., Jia, K., Song, X., Revhaug, I., Xia, H., and Zhu, Z.: Optimization of Causative Factors for Landslide Susceptibility Evaluation Using Remote Sensing and GIS Data in Parts of Niigata, Japan, PLoS One, 10, e0133262, https://doi.org/10.1371/journal.pone.0133262, 2015.

Evans, J. S., Oakleaf, J., Cushman, S. A., and Theobald, D.: An arc gis toolbox for surface gradient and geo-morphometric modeling, version 2.0-0., 2014.

780   Farooq, S. and Akram, M. S.: Landslide susceptibility mapping using information value method in Jhelum Valley of the Himalayas, Arabian Journal of Geosciences, 14, 824, https://doi.org/10.1007/s12517-021-07147-7, 2021.

Fawcett,   T.:   An   introduction   to   ROC   analysis,   Pattern   Recognit   Lett,   27,   861–874, https://doi.org/10.1016/j.patrec.2005.10.010, 2006.

Fell, R., Corominas, J., Bonnard, C., Cascini, L., Leroi, E., and Savage, W. Z.: Guidelines for landslide susceptibility, hazard
785   and risk zoning for land use planning, Eng Geol, 102, 85–98, https://doi.org/10.1016/j.enggeo.2008.03.022, 2008a.

Fell, R., Corominas, J., Bonnard, C., Cascini, L., Leroi, E., and Savage, W. Z.: Guidelines for landslide susceptibility, hazard and risk zoning for land-use planning, Eng Geol, 102, 99–111, https://doi.org/10.1016/j.enggeo.2008.03.014, 2008b.

Fressard, M., Thiery, Y., and Maquaire, O.: Which data for quantitative landslide susceptibility mapping at operational scale? Case study of the Pays d'Auge plateau hillslopes (Normandy, France), Natural Hazards and Earth System Sciences, 14, 569–
790   588, https://doi.org/10.5194/nhess-14-569-2014, 2014.

Gaidzik, K. and Ramírez-Herrera, M. T.: The importance of input data on landslide susceptibility mapping, Sci Rep, 11, 19334, https://doi.org/10.1038/s41598-021-98830-y, 2021.

Gorsevski, P. V, Gessler, P. E., Foltz, R. B., and Elliot, W. J.: Spatial Prediction of Landslide Hazard Using Logistic Regression and ROC Analysis, Transactions in GIS, 10, 395–415, https://doi.org/10.1111/j.1467-9671.2006.01004.x, 2006.

795   Guzzetti, F., Carrara, A., Cardinali, M., and Reichenbach, P.: Landslide hazard evaluation: a review of current techniques and their application in a multi-scale study, Central Italy, Geomorphology, 31, 181–216, https://doi.org/10.1016/S0169-555X(99)00078-1, 1999.

Guzzetti, F., Reichenbach, P., Ardizzone, F., Cardinali, M., and Galli, M.: Estimating the quality of landslide susceptibility models, Geomorphology, 81, 166–184, https://doi.org/10.1016/j.geomorph.2006.04.007, 2006a.

800 Guzzetti, F., Galli, M., Reichenbach, P., Ardizzone, F., and Cardinali, M.: Landslide hazard assessment in the Collazzone area, Umbria, Central Italy, Natural Hazards and Earth System Sciences, 6, 115–131, https://doi.org/10.5194/nhess-6-115-2006, 2006b.

Guzzetti, F., Mondini, A. C., Cardinali, M., Fiorucci, F., Santangelo, M., and Chang, K.-T.: Landslide inventory maps: New tools for an old problem, Earth Sci Rev, 112, 42–66, https://doi.org/10.1016/j.earscirev.2012.02.001, 2012.

805 Habumugisha, J. M., Chen, N., Rahman, M., Islam, M. M., Ahmad, H., Elbeltagi, A., Sharma, G., Liza, S. N., and Dewan, A.: Landslide Susceptibility Mapping with Deep Learning Algorithms, Sustainability, 14, 1734, https://doi.org/10.3390/su14031734, 2022.

Hastie, T., Tibshirani, R., and Friendman, J.: The Elements of Statistical Learning: Data Mining, Inference, and Prediction, Springer, New York, 2009.

810 Hemasinghe, H., Rangali, R. S. S., Deshapriya, N. L., and Samarakoon, L.: Landslide susceptibility mapping using logistic regression model (a case study in Badulla District, Sri Lanka), Procedia Eng, 212, 1046–1053, https://doi.org/10.1016/j.proeng.2018.01.135, 2018.

Ho, T.K.: Random decision forests, in: Proceedings of 3rd International Conference on Document Analysis and Recognition, 278–282, https://doi.org/10.1109/ICDAR.1995.598994, 1995.

815 Huang, F., Zhang, J., Zhou, C., Wang, Y., Huang, J., and Zhu, L.: A deep learning algorithm using a fully connected sparse autoencoder neural network for landslide susceptibility prediction, Landslides, 17, 217–229, https://doi.org/10.1007/s10346-019-01274-9, 2020a.

Huang, F., Cao, Z., Guo, J., Jiang, S.-H., Li, S., and Guo, Z.: Comparisons of heuristic, general statistical and machine learning models for landslide susceptibility prediction and mapping, Catena (Amst), 191, 104580,
820 https://doi.org/10.1016/j.catena.2020.104580, 2020b.

Huang, F., Tao, S., Li, D., Lian, Z., Catani, F., Huang, J., Li, K., and Zhang, C.: Landslide Susceptibility Prediction Considering Neighborhood Characteristics of Landslide Spatial Datasets and Hydrological Slope Units Using Remote Sensing and GIS Technologies, Remote Sens (Basel), 14, 4436, https://doi.org/10.3390/rs14184436, 2022.

Jacobs, L., Kervyn, M., Reichenbach, P., Rossi, M., Marchesini, I., Alvioli, M., and Dewitte, O.: Regional susceptibility
825 assessments with heterogeneous landslide information: Slope unit- vs. pixel-based approach, Geomorphology, 356, 107084, https://doi.org/10.1016/j.geomorph.2020.107084, 2020.

James, G., Witten, D., Hastie, T., and Tibshirani, R.: An Introduction to Statistical Learning, Springer, New York, 2013.

Jebur, M. N., Pradhan, B., and Tehrany, M. S.: Optimization of landslide conditioning factors using very high-resolution airborne laser scanning (LiDAR) data at catchment scale, Remote Sens Environ, 152, 150–165,
830 https://doi.org/10.1016/j.rse.2014.05.013, 2014.

Jurak, V., Ivan Matković, Miklin, Ž., and Snježana Mihalić: Data analysis of the landslides in the Republic of Croatia: Present state and perspectives, in: Landslides , 1923–1929, 1996.

Jurak, V., Ortolan, Ž., Ivšić, T., Herak, M., Šumanovac, F., Vukelić, I., Jukić, M. and Šurina, Z.: Geotehničko i seizmičko mikroniziranje grada Zagreba – pokušaji i ostvarenje (Geotechnical and seizmological microzonation of Zagreb City - attempts and accomplishments), in: Zbornik radova s konferencije razvitak Zagreba, Razvitak Zagreba, Zagreb, Croatia, 1-2 February 2008, 99-108, 2008. (in Croatian)

Kavzoglu, T., Sahin, E. K., and Colkesen, I.: Landslide susceptibility mapping using GIS-based multi-criteria decision analysis, support vector machines, and logistic regression, Landslides, 11, 425–439, https://doi.org/10.1007/s10346-013-0391-7, 2014.

Krkač, M., Bernat Gazibara, S., Sinčić, M., Lukačić, H., Šarić, G., and Snježana, M. A.: Impact of input dana on the quality of the landslide susceptibility large-scale maps: A case study from NW Croatia, in: Progress in Landslide Research and Technology, edited by: Alcántara-Ayala, I., Arbanas, Ž., Cuomo, S., Huntley D., Konagai, K., Mihalić Arbanas, S., Mikoš, M., Sassa, K., Tang, H., and Tiwari, B., 2023.

Landis, J.R. and Koch, G.G.: The measurement of observer agreement for categorical dana, Biometrics, 33 (1), 159-174, 1977

Lee, S.: Landslide susceptibility mapping using an artificial neural network in the Gangneung area, Korea, Int J Remote Sens, 28, 4763–4783, https://doi.org/10.1080/01431160701264227, 2007.

Mathew, J., Jha, V. K., and Rawat, G. S.: Weights of evidence modelling for landslide hazard zonation mapping in part of Bhagirathi valley, Uttarakhand, Curr Sci, 628–638, 2007.

Merghadi, A., Yunus, A. P., Dou, J., Whiteley, J., ThaiPham, B., Bui, D. T., Avtar, R., and Abderrahmane, B.: Machine learning methods for landslide susceptibility studies: A comparative overview of algorithm performance, Earth Sci Rev, 207, 103225, https://doi.org/10.1016/j.earscirev.2020.103225, 2020

Mihalić, S.: Recommendations for Landslide Hazard and Risk Mapping in Croatia, Geologia Croatica, 51(2), 195-204, https://doi.org/10.4154/GC.1998.15, 1988

Mihalić Arbanas, S., Bernat, S., Fabijanović, S., and Arbanas, Ž.: The analysis of historical landslide information from the area of the City of Zagreb and Primorsko-Goranska County, in: Proceedings of the 1st Regional Symposium on Landslides in the Adriatic-Balkan Region - Landslide and Flood Hazard Assessment, 91–96, 2014.

Mihalić Arbanas S, Krkač M, Bernat Gazibara S (2016) Application of advanced technologies in landslide research in the area of the City of Zagreb (Croatia, Europe), Geologica Croatica 69(2):179-192. http://doi.org/10.4154/gc.2016.18

Mihalić Arbanas, S., Bernat Gazibara, S., Krkač, M., Sinčić, M., Lukačić, H., Jagodnik, P., and Arbanas, Ž.: Landslide Detection and Spatial Prediction: Application of Data and Information from Landslide Maps, in: .) Progress in Landslide Research and Technology, Volume 1 Issue 2, edited by: Alcantara-Ayala, I., Arbanas, Ž., Huntley, D., Konagai, K., Mikoš, M., Sassa, K., Sassa, S., Tang, H. and Tiwari, B., Fullerton, CA, USA, 195–212, https://doi.org/10.1007/978-3-031-18471-0_16, 2023.

Miklin, Ž., Mlinar, Ž., Brkić, Ž., Hečimović, I., and Dolić, M.: Detailed engineering geological map of Podsljeme urbanised zone at a scale of 1:5 000 (DIGK-Phase I)., 2007.

Nefeslioglu, H. A., Gokceoglu, C., and Sonmez, H.: An assessment on the use of logistic regression and artificial neural networks with different sampling strategies for the preparation of landslide susceptibility maps, Eng Geol, 97, 171–191, https://doi.org/10.1016/j.enggeo.2008.01.004, 2008.

Neuhäuser, B. and Terhorst, B.: Landslide susceptibility assessment using "weights-of-evidence" applied to a study area at the Jurassic escarpment (SW-Germany), Geomorphology, 86, 12–24, https://doi.org/10.1016/j.geomorph.2006.08.002, 2007.

Neuhäuser, B., Damm, B., and Terhorst, B.: GIS-based assessment of landslide susceptibility on the base of the Weights-of-Evidence model, Landslides, 9, 511–528, https://doi.org/10.1007/s10346-011-0305-5, 2012.

Pascale, S., Parisi, S., Mancini, A., Schiattarella, M., Conforti, M., Sole, A., Murgante, B., and Sdao, F.: Landslide Susceptibility Mapping Using Artificial Neural Network in the Urban Area of Senise and San Costantino Albanese (Basilicata, Southern Italy), 473–488, https://doi.org/10.1007/978-3-642-39649-6_34, 2013.

Polak, K., Klemar, M., Nejkova, M., Radošević, N., Stepan, Z., Miroslav, M. and Križanić, Z.: Lithological analysis and categorisation of terrain according to soil stability of Medvednica slopes in the area of the City of Zagreb, Geotehnika-Geoexpert, Zagreb, 102, 1979 (in Croatian)

Petschko, H., Bell, R., and Glade, T.: Effectiveness of visually analyzing LiDAR DTM derivatives for earth and debris slide inventory mapping for statistical susceptibility modeling, Landslides, 13, 857–872, https://doi.org/10.1007/s10346-015-0622-1, 2016.

Pourghasemi, H. R., Sadhasivam, N., Amiri, M., Eskandari, S., and Santosh, M.: Landslide susceptibility assessment and mapping using state-of-the art machine learning techniques, Natural Hazards, 108, 1291–1316, https://doi.org/10.1007/s11069-021-04732-7, 2021.

Pradhan, B.: A comparative study on the predictive ability of the decision tree, support vector machine and neuro-fuzzy models in landslide susceptibility mapping using GIS, Comput Geosci, 51, 350–365, https://doi.org/10.1016/j.cageo.2012.08.023, 2013.

Ray, R.L., Lazzari, M., and Olutimehin, T.: Remote Sensing Approaches and Related Techniques to Map and Study Landslides, in: Landslides - Investigation and Monitoring, IntechOpen, https://doi.org/10.5772/intechopen.93681, 2020.

Razak, K. A., Santangelo, M., Van Westen, C. J., Straatsma, M. W., and de Jong, S. M.: Generating an optimal DTM from airborne laser scanning data for landslide mapping in a tropical forest environment, Geomorphology, 190, 112–125, https://doi.org/10.1016/j.geomorph.2013.02.021, 2013.

Reichenbach, P., Rossi, M., Malamud, B. D., Mihir, M., and Guzzetti, F.: A review of statistically-based landslide susceptibility models, Earth Sci Rev, 180, 60–91, https://doi.org/10.1016/j.earscirev.2018.03.001, 2018.

Rossi, M., Guzzetti, F., Reichenbach, P., Mondini, A. C., and Peruccacci, S.: Optimal landslide susceptibility zonation based on multiple forecasts, Geomorphology, 114, 129–142, https://doi.org/10.1016/j.geomorph.2009.06.020, 2010.

Rossi, M., Bornaetxea, T., and Reichenbach, P.: LAND-SUITE V1.0: a suite of tools for statistically based landslide susceptibility zonation, Geosci Model Dev, 15, 5651–5666, https://doi.org/10.5194/gmd-15-5651-2022, 2022.

Sandić, C., Marjanović, M., Abolmasov, B., and Tošić, R.: Integrating landslide magnitude in the susceptibility assessment of the City of Doboj, using machine learning and heuristic approach, J Maps, 19, https://doi.org/10.1080/17445647.2022.2163199, 2023.

Sarkar, S., Roy, A. K., and Martha, T. R.: Landslide susceptibility assessment using Information Value Method in parts of the Darjeeling Himalayas, Journal of the Geological Society of India, 82, 351–362, https://doi.org/10.1007/s12594-013-0162-z, 2013.

Scaioni, M., Longoni, L., Melillo, V., and Papini, M.: Remote Sensing for Landslide Investigations: An Overview of Recent Achievements and Perspectives, Remote Sens (Basel), 6, 9600–9652, https://doi.org/10.3390/rs6109600, 2014.

Shirvani, Z.: A Holistic Analysis for Landslide Susceptibility Mapping Applying Geographic Object-Based Random Forest: A Comparison between Protected and Non-Protected Forests, Remote Sens (Basel), 12, 434, https://doi.org/10.3390/rs12030434, 2020.

Sinčić, M., Bernat Gazibara, S., Krkač, M., Lukačić, H., and Mihalić Arbanas, S.: The Use of High-Resolution Remote Sensing Data in Preparation of Input Data for Large-Scale Landslide Hazard Assessments, Land (Basel), 11, 1360, https://doi.org/10.3390/land11081360, 2022a.

Sinčić, M., Bernat Gazibara, S., Krkač, M., and Mihalić Arbanas, S.: Landslide susceptibility assessment of the City of Karlovac using the bivariate statistical analysis, Rudarsko-geološko-naftni zbornik, 37, 149–170, https://doi.org/10.17794/rgn.2022.2.13, 2022b.

Soeters, R. and van Westen, C. J.: Slope Instability Recognition Analysis and Zonation, in: Landslides: Investigation and Mitigation, edited by: Turner, K. T. and Schuster, R. L., Washington DC, 129–177, 1996.

State Geodetic Administration, WMS server, topographic map: https://geoportal.dgu.hr/services/tk/wms, last access: 6 February 2024.

Šikić, V.: Engineering geology of Zagreb - north and south, 1967.

Šikić, K., Basch, O., and Šimunić, A.: Basic Geological Map, scale 1:100 000, Zagreb sheet, 1972.

Šikić, K., Basch, O., and Šimunić, A.: Geological notes for Basic geological map, scale 1:100 000, Zagreb sheet, 1979.

Tehrany, M. S., Pradhan, B., and Jebur, M. N.: Spatial prediction of flood susceptible areas using rule based decision tree (DT) and a novel ensemble bivariate and multivariate statistical models in GIS, J Hydrol (Amst), 504, 69–79, https://doi.org/10.1016/j.jhydrol.2013.09.034, 2013.

Tehrany, M. S., Pradhan, B., and Jebur, M. N.: Flood susceptibility mapping using a novel ensemble weights-of-evidence and support vector machine models in GIS, J Hydrol (Amst), 512, 332–343, https://doi.org/10.1016/j.jhydrol.2014.03.008, 2014.

Tyagi, A., Tiwari, R. K., and James, N.: Mapping the landslide susceptibility considering future land-use land-cover scenario, Landslides, 20, 65–76, https://doi.org/10.1007/s10346-022-01968-7, 2023.

930 Vakhshoori, V. and Zare, M.: Is the ROC curve a reliable tool to compare the validity of landslide susceptibility maps?, Geomatics, Natural Hazards and Risk, 9, 249–266, https://doi.org/10.1080/19475705.2018.1424043, 2018.

van Westen, C. J., van Duren, I., Kruse, H. M. G., and Terlien, M. T. J.: Training Package for Geographic Information Systems in Slope Stability Zonation, Part 1: Theory, ITC Publication, Eeschede, 1993.

van Westen, C. J.: Use of weights of evidence modeling for landslide susceptibility mapping, 2002.

935 van Westen, C. J., Rengers, N., and Soeters, R.: Use of Geomorphological Information in Indirect Landslide Susceptibility Assessment, Natural Hazards, 30, 399–419, https://doi.org/10.1023/B:NHAZ.0000007097.42735.9e, 2003.

van Westen, C. J., Castellanos, E., and Kuriakose, S. L.: Spatial data for landslide susceptibility, hazard, and vulnerability assessment: An overview, Eng Geol, 102, 112–131, https://doi.org/10.1016/j.enggeo.2008.03.010, 2008.

Vapnik, V. N.: The Nature of Statistical Learning Theory, Springer New York, New York, NY, https://doi.org/10.1007/978-

940 1-4757-2440-0, 1995.

Vojteková, J. and Vojtek, M.: Assessment of landslide susceptibility at a local spatial scale applying the multi-criteria analysis and GIS: a case study from Slovakia, Geomatics, Natural Hazards and Risk, 11, 131–148, https://doi.org/10.1080/19475705.2020.1713233, 2020.

Wang, L.-J., Guo, M., Sawada, K., Lin, J., and Zhang, J.: A comparative study of landslide susceptibility maps using logistic

945 regression, frequency ratio, decision tree, weights of evidence and artificial neural network, Geosciences Journal, 20, 117–136, https://doi.org/10.1007/s12303-015-0026-1, 2016a.

Wang, Q., Li, W., Wi, Y., Pei, Y., Xing, M., and Yang, D.: A comparative study on the landslide susceptibility mapping using evidential belief function and weights of evidence models, Journal of Earth System Science, 125, 645–662, https://doi.org/10.1007/s12040-016-0686-x, 2016b.

950 Wang, G., Chen, X., and Chen, W.: Spatial Prediction of Landslide Susceptibility Based on GIS and Discriminant Functions, ISPRS Int J Geoinf, 9, 144, https://doi.org/10.3390/ijgi9030144, 2020.

Wang, H., Zhang, L., Luo, H., He, J., and Cheung, R. W. M.: AI-powered landslide susceptibility assessment in Hong Kong, Eng Geol, 288, 106103, https://doi.org/10.1016/j.enggeo.2021.106103, 2021.

Xiao, T., Yu, L., Tian, W., Zhou, C., and Wang, L.: Reducing Local Correlations Among Causal Factor Classifications as a

955 Strategy to Improve Landslide Susceptibility Mapping, Front Earth Sci (Lausanne), 9, https://doi.org/10.3389/feart.2021.781674, 2021.

Xing, Y., Yue, J., Guo, Z., Chen, Y., Hu, J., and Travé, A.: Large-Scale Landslide Susceptibility Mapping Using an Integrated Machine Learning Model: A Case Study in the Lvliang Mountains of China, Front Earth Sci (Lausanne), 9, https://doi.org/10.3389/feart.2021.722491, 2021.

960 Yan, G., Liang, S., Gui, X., Xie, Y., and Zhao, H.: Optimizing landslide susceptibility mapping in the Kongtong District, NW China: comparing the subdivision criteria of factors, Geocarto Int, 34, 1408–1426, https://doi.org/10.1080/10106049.2018.1499816, 2019.

Yao, X., Tham, L. G., and Dai, F. C.: Landslide susceptibility mapping based on Support Vector Machine: A case study on natural slopes of Hong Kong, China, Geomorphology, 101, 572–582, https://doi.org/10.1016/j.geomorph.2008.02.011, 2008.

965 Yin, K. L. and Yan, T. Z.: Statistical prediction model for slope instability of methamorphosed rocks, in: Proceedings of Fifth International Symposium on Landslides, 1269–1272, 1988.

Yusof, N. M., Pradhan, B., Shafri, H. Z. M., Jebur, M. N., and Yusoff, Z.: Spatial landslide hazard assessment along the Jelapang Corridor of the North-South Expressway in Malaysia using high resolution airborne LiDAR data, Arabian Journal of Geosciences, 8, 9789–9800, https://doi.org/10.1007/s12517-015-1937-x, 2015.

970 Zêzere, J. L., Pereira, S., Melo, R., Oliveira, S. C., and Garcia, R. A. C.: Mapping landslide susceptibility using data-driven methods, Science of The Total Environment, 589, 250–267, https://doi.org/10.1016/j.scitotenv.2017.02.188, 2017.

Zhao, X. and Chen, W.: Optimization of Computational Intelligence Models for Landslide Susceptibility Evaluation, Remote Sens (Basel), 12, 2180, https://doi.org/10.3390/rs12142180, 2020.